THESIS FOR THE DEGREE OF DOCTOR OF PHILOSOPHY

Thermo-mechanical behaviour of pearlitic railway steels

ERIKA STEYN

Department of Industrial and Materials Science

CHALMERS UNIVERSITY OF TECHNOLOGY

Gothenburg, Sweden 2024

Thermo-mechanical behaviour of pearlitic railway steels
ERIKA STEYN
ISBN: 978-91-8103-045-7

Doktorsavhandlingar vid Chalmers tekniska högskola
Ny serie nr. 5503
ISSN 0346-718X

Department of Industrial and Materials Science
Division of Engineering Materials
Chalmers University of Technology
SE-412 96 Gothenburg
Sweden
Telephone + 46 (0)31-772 1000

Cover:
An SEM image of the pearlitic microstructure as seen in railway wheel steel ER7T that has been spheroidised to some extent (top), and the corresponding image quantification results (bottom) as discussed in Paper II. See Figure 20 for scale bar.

Printed by Chalmers Reproservice
Gothenburg, Sweden 2024

Thermo-mechanical behaviour of pearlitic railway steels

ERIKA STEYN
Department of Industrial and Materials Science
Chalmers University of Technology

Abstract

Railway operations and maintenance activities typically involve high levels of localised stresses and temperatures. The material behaviour of common pearlitic railway steels has previously been studied under thermal and different mechanical loadings, respectively. However, in service the material occasionally experiences these loads simultaneously, which results in a complex thermo-mechanical loading. This thesis attempts to characterise the material behaviour of rail and railway wheel steel when exposed to thermo-mechanical loads. The effect of localised heating events is studied, and the influence of process parameters are investigated.

This thesis work encompasses both slow and rapid local heating events, with the objective of investigating changes in the mechanical behaviour, microstructure and residual stress states. A slow heating cycle was employed to simulate severe block braking on railway wheel material. This was studied through thermo-mechanical cycling to peak temperatures varying between 300 °C and 650 °C, while the thermal dilatation was restricted to different degrees between free expansion and full restriction. Rapid heating and cooling events were studied by using laser heating. Laser sources from PBF-LB additive manufacturing equipment and laser welding equipment were used to simulate local heating events.

It was seen that thermo-mechanical loads result in strongly temperature-dependent material behaviour; however, the effect most notable is the resulting residual stress state in the material after testing. For the slow thermal cycles, as experienced during severe block braking, it can be concluded that overheating of the wheel rim does not have severe consequences for the mechanical properties of the wheel. Quantification of spheroidisation in the wheel rim showed that increased loads at these high temperatures could have a beneficial effect on the material properties. This thesis work made use of novel approaches, such as the laser heating experiments, that can be useful to simulate also other local heating events and thereby characterise the material behaviour.

The findings presented in this thesis provide insight into the material behaviour of railway steels during local heating events under conditions similar to those observed in practice. These insights can be used to inform railway wheel design, rail and wheel maintenance procedures, and component replacement limits. Furthermore, the work has been implemented and used for verification of simulations in parallel activities and provide an experimental basis for the further development of predictive models.

keywords: railway wheel steel, pearlitic microstructure, spheroidisation, martensite, thermo-mechanical behaviour, residual stress, laser heating

For my dad.

My role model, mentor and friend.

He taught me to live life to the fullest, and believed in me even when I didn't.

Preface

The research presented in this thesis is carried out at the Department of Industrial and Materials Science at Chalmers University of Technology between June 2019 and May 2024. The research project MU36, "Material characteristics in welding and other local heating events", is part of the ongoing activities within the National Centre of Excellence CHARMEC – Chalmers Railway Mechanics (www.chalmers.se/charmec). The study has been partially funded from the European Union's Horizon 2020 research and innovation programmes in the projects In2Track2 and In2Track3 under grant agreement numbers 826255 and 101012456, as well as in the Europe Rail project IAM4RAIL under grant agreement No. 101101966.

Overview of appended papers

Paper I **Thermo-mechanical response of near-pearlitic steel heated under restriction of thermal expansion.** E. Steyn, J. Ahlström. *Submitted for international publication*.

Author contribution: Planning, execution, and analysis of TMF experiments. Performed subsequent room temperature hardness testing and microstructural analysis. Responsible for the planning, writing and submission of the research paper.

Summarised abstract: This study explores the effect of thermo-mechanical loadings on railway wheel steel, conducting thermal cycling at various peak temperatures and thermal dilatation restriction levels. Findings reveal complex material behaviour, impacting residual stresses in overheated wheels and potentially influencing fatigue properties. The research enhances understanding of thermo-mechanical behaviour in railway steels, aiding in the development of material models necessary for the simulation and prediction of severe block braking.

Paper II **The effect of thermo-mechanical loading on the microstructure evolution in near-pearlitic steel**. E. Steyn, J. Ahlström. In manuscript

Author contribution: Planning, execution, and analysis of TMF experiments. Development of spheroidisation quantification code. Performed subsequent room temperature hardness testing and. microstructural analysis. Performed SEM microscopy and spheroidisation quantification, and statistical analysis of results. Responsible for the planning and writing of the research paper.

Summarised abstract: This paper aims to identify the link between thermo-mechanical loading and microstructural evolution in near-pearlitic railway wheel steel. Thermo-mechanical testing with peak temperatures of 300 °C and 650 °C is considered for this study. In previous studies it has been shown that spheroidisation of pearlite increases significantly

with an increase in temperature. However, microstructural evaluation of isolated regions proved insufficient to comment on the degree of spheroidisation; therefore, microstructural characterisation was performed using scanning electron microscopy and quantification using an in-house developed code. Hardness and spheroidisation quantification results for the wheel rim material showed that this fine-pearlitic microstructure is sensitive to the degree of thermal dilatation restriction during cycling to a peak temperature of 650 °C. This can have significant implications for tread braking operations and could prove beneficial for any applications of pearlitic steels exposed to static and dynamic thermo-mechanical loading to peak temperatures in the spheroidisation range.

Paper III **Thermomechanical testing and modelling of railway wheel steel.** E. Voortman Landström, E. Steyn, J. Ahlström, T. Vernersson. *Int. Journal of Fatigue*. 2023.

Author contribution: Planned the TMF test cycles and ratchetting tests in dialogue with the co-authors and executed the experiments (as described in Papers I and II). Planned and executed subsequent room temperature hardness testing and heat treatment. Contributed to writing of the paper, with focus on the materials and experimental sections.

Summarised abstract: Computational models simulating the thermo-mechanical behaviour of railway wheels are generally based on laboratory test results that do not reflect actual in-service scenarios. Studies of tread braking suggest that temperatures in the wheel tread can exceed 600°C, which will significantly affect the mechanical properties of the material. Previous studies were limited to isothermal testing for calibrating constitutive material models; in this paper, an existing model is extended to capture the thermo-mechanical behaviour as well.

Paper IV **Thermal pulses on pearlitic steels: Influence of laser scanning parameters on surface layers transforming to martensite.** E. Steyn, B. Andersson, J. Ahlström. *Submitted to Journal of Materials Processing Technology*.

Author contribution: Planned and executed the experiments and experimental analysis including residual stress measurements, room temperature hardness and microscopy. Responsible for the planning, writing and submission of the research paper.

Summarised abstract: The impact of rapid local surface heating and cooling is studied on railway steels using equipment for both laser-based additive manufacturing and laser welding. The fully pearlitic high carbon rail steel, R260, is compared to the near-pearlitic medium carbon railway wheel steel, ER7T. It is shown that, despite the complex correlations between process parameters, microstructure, and residual stresses, outcomes can be predicted for the variation of single parameters. Complementary numerical simulations, validated by experimental measurements, provide insight into the relationship between thermal strains

and martensite transformation. The results indicate that the methods are comparable and could potentially enhance the simulation of maintenance processes.

Paper V **Martensite formation due to thermal loading during rail grinding on pearlitic rail steel.** E. Steyn, J. Ahlström. *In manuscript.*

Author contribution: Planned and supported the experiments and experimental analysis. Responsible for planning and writing the manuscript to be submitted as short communication.

Summarised abstract: Pearlitic rail steels are susceptible to martensite formation in the surface layer due to rapid cooling after exposure to high temperatures above the austenitisation temperature. The high thermal power imposed during rail grinding operations can result in the formation of a thin layer of martensite, called a white etching layer (WEL). This experimental grinding study aims to investigate the thermal impact of rail grinding in a realistic laboratory setup. The influence of applied power and grinding speed parameters during grinding operations on the microstructure of the altered surface layer were investigated on two rail steel grades (R260 and R350HT). The grinding experiments demonstrated very small differences in transformed depth between the two rail grades, and the martensite hardness is similar. In transitions between facets, tempering of the martensite occurs that inevitably decreases the hardness locally. Increasing the feed rate, drastically decreases the depth of the transformed layer.

Paper VI **Rail machining – current practices and potential for optimisation**. E. Steyn, B. Paulsson, A. Ekberg, E. Kabo. *Proceedings of the Institution of Mechanical Engineers, Part F: Journal of Rail and Rapid Transit.* 2024;238(2):196-205

Author contribution: Researching current and best practices of rail machining and the effect on the rail material. Collaboration in discussions with international infrastructure managers to determine the state of the art and the current knowledge gaps. Participated in outlining and writing the paper.

Summarised abstract: Investigate current rail machining practices, examining the objectives and consequences of noncompliance. The potential detrimental effects of rail machining and how to minimise them are discussed to identify the reasons for this and to suggest strategies to further optimise rail machining. This study identifies opportunities to improve rail machining, and highlights limitations due to a lack of knowledge and current predictive models. This prevents quantifying benefits of innovative solutions and complicates the transfer of knowledge between laboratory studies and operational conditions in practice.

Reports/ papers not appended to this thesis:

A.1 **Simulation-Based Assessment of Railhead Repair Welding Process Parameters.** B. Andersson; E. Steyn; M. Ekh; L.B. Josefson. Submitted to Welding in the World

A.2 **In2Track3 D3.1 – section 2.1.3. Rail machining strategies.** E. Steyn, B. Paulsson, A. Ekberg. *Deliverable Report for In2Track3. 2022.*

A.3 **Simulation of repair welding on pearlitic railway steel using additive manufacturing equipment.** E. Steyn, J. Ahlström. Proceedings of the *12th International Conference on Contact Mechanics and Wear of Rail/Wheel Systems, Melbourne, Australia, 2022*

List of abbreviations and acronyms

AM	Additive manufacturing
BCC	body-centered cubic (crystal structure)
BCT	body-centered tetragonal (crystal structure)
DSA	Dynamic strain aging
EDM	Electric discharge machining
EU	European Union
FCC	face-centered cubic (crystal structure)
FEGSEM	Field emission gun scanning electron microscope
LB-PBF	Laser-based powder bed fusion
LCC	Life cycle cost
LCF	Low cycle fatigue
LW	Laser welding
MMA	Manual metal arc welding
RCF	Rolling contact fatigue
SAW	Submerged arc welding
SEM	Scanning electron microscope/ microscopy
TMF	Thermo-mechanical fatigue
XRD	X-ray diffraction
ZST(E)	Zero-stress test/ Zero-stress test evaluation
ZTS	Zero total strain

Table of contents

INTRODUCTION

1.1. A foundation for sustainable transport

Rail transport has been in existence for over 6 000 years, with evidence of wooden tracks dating back to the Neolithic period [1]. The industrial revolution marked a significant shift from manual and animal-powered transportation to steam-powered carriages and commercial railways made of steel. During the 19th century, rapid developments in locomotive power, railway design and materials led to the growth of a global railway network, further fuelled by advances in electrification, steelmaking practices and competition for the fastest trains.

Given the current global emphasis on sustainability, there is a growing focus on advancements in rail transport. Emerging technologies like hydrogen-powered trains are promising, while new lines are being constructed and existing networks are constantly expanded and developed. Therefore, it is important to properly maintain both new and existing infrastructure to ensure the sustainability of the global rail network.

In 2019, 52 % of all goods in the EU were transported by road, compared to only 12 % by rail; only 7 % of European travel was by train [2]. The transport sector is responsible for almost a third of EU greenhouse gas emissions, with rail contributing just 0.4 % [2,3]. As part of the European Green Deal [4], the European Union (EU) has committed to a 55 % reduction in carbon emissions by 2030 and carbon neutrality by 2050. To achieve this, transport emissions must be reduced by 90 %.

The development of a sustainable trans-European rail network is a key initiative with the main objectives to triple high-speed rail and double rail freight traffic. This development will be a quick win in terms of emission reduction targets. Infrastructure improvements and expansion should focus on reducing life cycle costs (LCC) and improving end-user affordability [3,5].

However, developing infrastructure poses technical challenges, such as increasing demands on the quality and frequency of maintenance required, while reducing maintenance time. To improve traffic management and maintenance activities, standardisation and improved predictive models can be utilised. Programmes like Horizon Europe provide the resources and framework for research and development necessary to achieve these milestones, overcome challenges, and facilitate collaboration between industry and academic partners in various research areas [5].

1.2. Project background

To guarantee a sustainable rail network, it is essential to implement effective maintenance techniques. Strategies to restore damaged or worn rail-wheel contact surfaces include both subtractive surfacing

techniques, such as rail grinding and milling and machining (turning) of wheel tread surfaces, and additive techniques, such as repair welding. However, localised heating alters the local mechanical properties and residual stresses, which could counteract the beneficial properties introduced during manufacturing. Similarly, localised heating events during operation, such as friction in the wheel-rail contact area during braking, can cause thermal damage like that observed during heat-inducing maintenance processes. The effects of thermal damage on mechanical and microstructural properties of repaired sections are not fully understood.

Local heating events in pearlitic railway steels can cause phase transformations, resulting in different temperature-dependent properties such as thermal expansion, density, or mechanical properties. These transformations can lead to residual stresses or localised strains during subsequent loading, potentially causing defects in the rail and wheel surfaces which in turn can lead to fatigue damage and an increased need for maintenance.

Maintenance strategies aim to increase component life and minimise the life cycle cost (LCC). The heat input can be controlled by optimising the process parameters of conventional repair methods. This can achieve beneficial heat treatment, resulting in the desired microstructures and mechanical properties in the repaired component. New repair methods, such as laser welding and additive manufacturing, are rapidly evolving through continuous research and testing. However, scientific evidence must prove these new technologies as superior before they can replace existing and proven repair methods.

Previous studies have investigated the behaviour of pearlitic steels after exposure to plastic straining and elevated temperatures respectively, and the combination of strain and temperature for the isothermal case. The results offer valuable insights into the effects of various thermal processes, including rail surfacing techniques [6,7], rail welding [8–10], laser cladding [11,12], and contact friction heating [13–18]. Combining different research areas provide new insights that may improve predictive models of thermal processes during rail operations and maintenance.

1.3. Aim and research objectives

The aim of this research is to characterise the material behaviour of rail and railway wheel steel during high temperature processes, with particular reference to combined thermal and mechanical loading and the influence of process parameters.

The main objectives include:

- Experimentally simulating the effect of severe block braking on near-pearlitic railway wheel steel (ER7T) behaviour and microstructure by exposing material to various thermo-mechanical loading cycles with different peak temperatures and degrees of restriction of thermal dilatation.

- Characterisation of the effect of rapid local heating and cooling events on the microstructure and residual stress state, comparing near-pearlitic railway wheel steel (ER7T) and pearlitic rail steel (R260).
- Review the implications of maintenance processes of pearlitic railway steel regarding deterioration due to thermal and thermo-mechanical loads.

This research will expand on the current understanding of pearlitic material behaviour during local heating events. The findings may contribute to the development of improved maintenance guidelines and more accurate predictive models of high-temperature thermo-mechanical processes. This thesis presents the theoretical background and work performed during the research project. Section 2 provides an overview of typical railway materials, while Section 3 outlines the degradation mechanisms and maintenance techniques used in the railway industry. Section 4 focuses on the research methodology used to obtain the results presented in the appended papers, as summarised and discussed in Section 5. Finally, Section 6 provides main conclusions and possible future work.

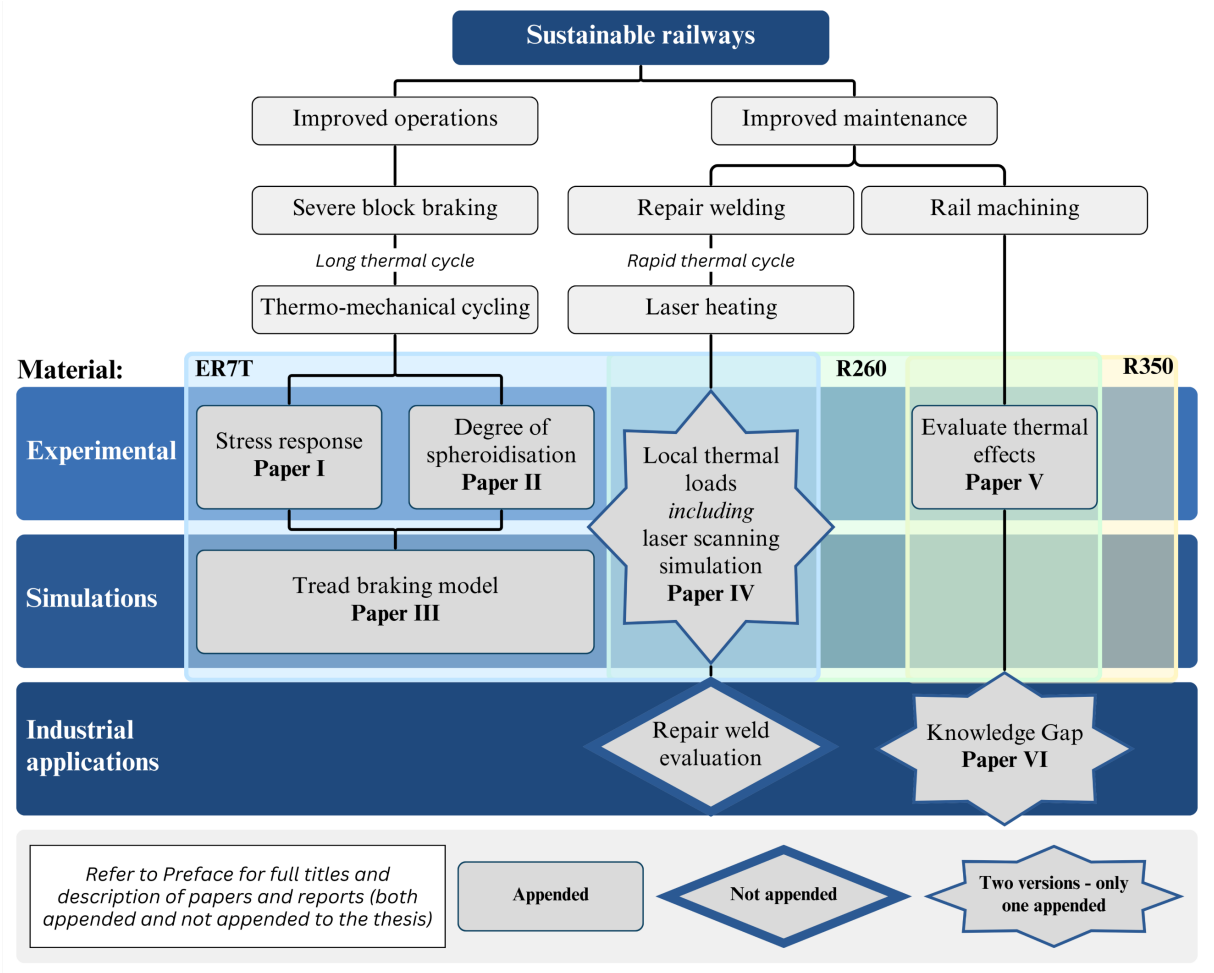

***Figure 1**: Relationship between appended papers*

RAILWAY MATERIALS

2.1. Pearlitic steels in railways

Pearlitic steels have a wide range of applications, from high-strength bolts [19] to piano wire, cables for suspension bridges and the steel-cord reinforcement in tyres [20–22]. Pearlitic and near-pearlitic steels are commonly used in the railway industry for the production of railway wheel and rails.

The work presented in this thesis is performed predominantly on railway wheel steel ER7 and rail steel R260. Although there are some compositional differences between these two materials, as seen in Table 1, both feature the pearlitic microstructure of interest. The investigation of thermo-mechanical material behaviour can benefit both the rail and railway wheel industries. It is beneficial to compare these materials – not only can new research and established principles be applied to both fields, but these learnings can be used to improve simulations and best-practices on both rails and railway wheels.

***Table 1**: Chemical composition (maximum wt%) of common railway materials* [23,24]

Element [wt%, max]	C	Si	Mn	Mo [1,2,3]	Cr [1,2]	Ni [1,2,3]	S	P	V	Cu [2,3]	Al	N	Fe	Sn [3]	Sb [3]	Ti [3]	Nb [3]	H [4,5]
ER7	0.52	0.40	0.80	0.08	0.30	0.30	0.015	0.02	0.06	0.30	-	-		-	-	-	-	2.50
ER8	0.56	0.40	0.80	0.08	0.3	0.30	0.015	0.02	0.06	0.30	-	-		-	-	-	-	2.50
R260 [6]	0.82	0.60	1.25	0.02	0.15	0.10	0.03	0.03	0.03	0.15	0.004	0.01		0.03	0.02	0.025	0.01	2.50
R350HT	0.82	0.60	1.25	0.02	0.15	0.10	0.03	0.025	0.03	0.15	0.004	0.01		0.03	0.02	0.025	0.04	2.50

1. For ER7 and ER8: Mo, Cr and Ni combined cannot exceed 0.5 wt%
2. For R260 and R350HT: Cr, Mo, Ni, Cu and V combined cannot exceed 0.35 wt% for R260 and 0.25 wt% for R350HT respectively.
3. Mo, Ni, Cu, Sn, Sb, Ti and Nb are considered residual elements in rail steels R260 and R350HT. Here, the following also applies: (Cu + 10 Sn) ≤ 0.35 wt %
4. Unit: ppm (10^{-6}) by mass, maximum.
5. These values apply to category 2 wheels as defined in EN 13262. For category 1 wheels (traffic speed >200 km/h), this is reduced to 2.00.
6. This compositional data is valid for all rail profiles over 27 kg/m. However, EN 13674 Part 1 (rails 46 kg/m and heavier) have an additional requirement that oxygen content cannot exceed 0.002 % (ppm) by mass.

Railway wheels are commonly made from hypo-eutectoid medium carbon steels. In Europe, the most common grades are ER7 and ER8, with the standardised compositions according to EN 13262 shown in Table 1, although other grades are also used in different regions [23,25,26]. ER7 is suitable for most applications, especially block braked wheels, whereas ER8 is typically used in high-demand applications [23,27].

Medium and high carbon steels with similar compositions are used globally for railways; however, the designations and preferences often differ between infrastructure managers. Various rail grades are used throughout Europe. Although the use of heat treated (so-called premium) rail grades are becoming more common and bainitic variants are being studied, the standard pearlitic R260 rail grade is still widely used. This is considered the economic choice for straight track and areas where only light rolling contact fatigue (RCF) and wear is expected [28]. Heat treated rail grades like R350HT are suitable for use in light rail (e.g. metro lines), mixed and high-speed traffic. It has also been proven beneficial in curves with a radius of up to 5 000 m where higher degrees of wear and RCF are

expected [29]. EN 13674 is used to standardise the European rail grades – Table 1 shows the standard chemical composition for the R260 and R350HT rail grades [24,30].

2.2. Microstructures of interest

2.2.1. Pearlite

Morphology and formation

Pearlite is a common microstructure forming in steels when austenite with an FCC crystal structure transforms during cooling into a two-phase microstructure – this microstructure consists of ferrite with a BCC crystal structure and cementite (Fe_3C) with an FCC crystal structure. Austenite with a eutectoid chemical composition will form a fully lamellar pearlitic microstructure – the ferrite and cementite lamellae will grow side-by-side from the austenite grain boundaries. This results in different pearlite colonies forming within the original austenitic grain, each with its own distinct orientation [31].

Pearlite colonies can form by the nucleation of either cementite or ferrite, depending on the composition of the material. Lamellar growth occurs by carbon diffusion in the austenite – the formation of cementite lamellae results in carbon depletion in the surrounding ferrite, which in turn increases the driving force for ferrite nucleation. The growing ferrite lamellae rejects carbon, which then diffuses to the austenite-cementite interface of neighbouring growing cementite lamellae [31–33]. This interdependency results in the uniform growth of the pearlite colony; however, the size of the lamellae is highly dependent on the degree of undercooling. Slow cooling rates (i.e. a low degree of undercooling) allow for carbon to diffuse over longer distances, forming coarse pearlite that has larger interlamellar spacing (ISP). Increasing the cooling rate effectively limits the distance that carbon will diffuse and results in a finer pearlitic microstructure, i.e. having a smaller ISP. A pearlitic microstructure can also be obtained by isothermal decomposition of austenite, where the material is quenched to below the eutectoid temperature (A_{C1}) and held isothermally until the austenite is fully transformed.

Railway wheel steel ER7T is a hypo-eutectoid steel with 0.52 wt% (max) carbon, where some ferrite forms before the eutectoid reaction occurs. This pro-eutectoid ferrite (or free ferrite) is clearly distinguishable (see Figure 2). Forced cooling during the production of railway wheels (see Section 3.1.1) results in rapid decomposition of austenite, which inhibits the formation of free ferrite. Therefore, these railway wheel materials have a near-pearlitic microstructure with only about 10 % free ferrite close to the rim-chilled virgin wheel surface; this is slightly higher for the ER7 material [34]. Rail steel R260, a eutectoid steel with 0.82 wt% (max) carbon, transforms completely to pearlite upon cooling.

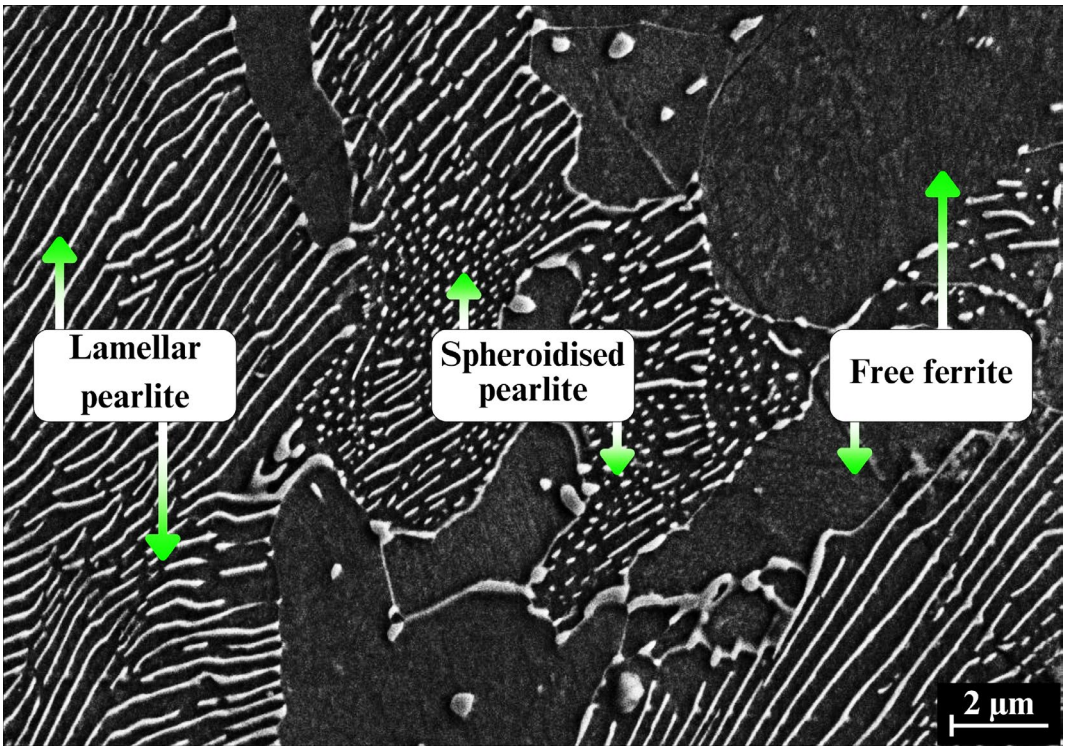

***Figure 2**: Features in the pearlitic microstructure of railway wheel steel ER7*

Spheroidised pearlite

Spheroidised pearlite (*also called spheroidite or globularised pearlite*) can form when lamellar pearlite is exposed to elevated temperatures, just below the eutectoid transformation temperature A_1. An increase in atom mobility (diffusion) due to increasing temperature results in the two-phase microstructure to spheroidise the minor phase; in this case, cementite [35]. Since the surface area of a sphere is the smallest possible per confined unit volume, the decrease in surface energy drives the spheroidisation process in pearlite. Other studies have also shown that the degree of spheroidisation is both time and temperature dependent [35–38].

The pearlitic microstructure is idealised as planar and evenly distributed lamellae. In reality the cementite lamellae are often curved and discontinuous, with gaps or holes [39] as shown in Figure 3(a) and (b) below. According to the fault migration theory [40], these curved regions or discontinuities have higher chemical potential and can act as initiation sites for spheroidisation. Discontinuities can also be formed by plastic deformation [41], suggesting that the combination with elevated temperatures could lead to a higher tendency for spheroidisation. During spheroidisation, the cementite lamellae break apart into smaller flakes or pieces as shown in Figure 3(c), which coarsens to form spheroids.

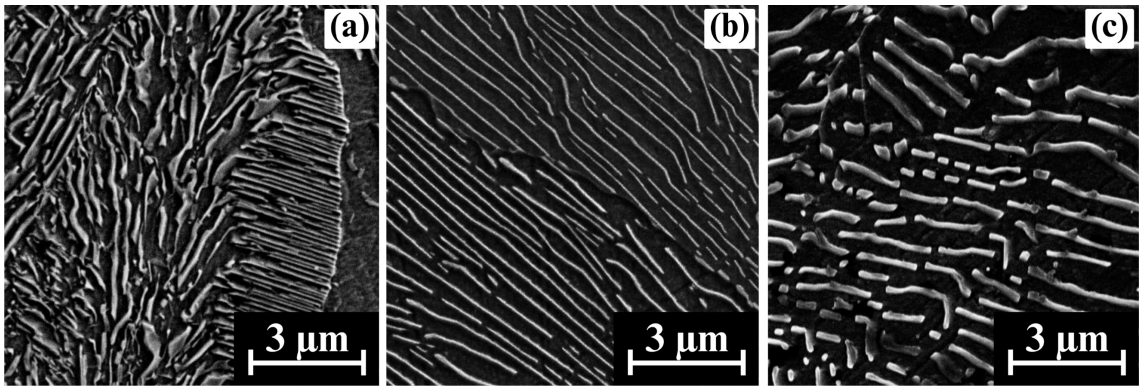

Figure 3*: Curved lamellae and discontinuities can act as initiation points for spheroidisation.* ***(a)*** *Irregular shaped pearlitic lamellae* ***(b)*** *Curved pearlitic lamellae with discontinuities* ***(c)*** *Cementite lamellae start to break apart before it coarsens into spheroids*

2.2.2. Martensite

Martensitic transformation is a rapid, diffusionless process which can occur in steel when it is quenched from the austenitic phase to room temperature [35,42]. An increase in carbon content lowers the temperature at which martensite starts to form (M_s) [31] – it is shown in **Paper IV** that ER7 steel with 0.52 wt% carbon has an M_s of about 285 °C, while the M_s is about 161 °C for R260 with 0.82 wt% carbon. A similar decrease is seen for the temperature at which the transformation is complete (M_f): 164 °C for ER7 compared to 22 °C for R260. At high carbon content, specifically for hyper-eutectoid steels, not all austenite is transformed to martensite after cooling to room temperature. This *retained austenite* should be considered during heat treatment design, as it can transform to martensite or pearlite during subsequent heating cycles. Unwanted dimensional changes and additional residual stresses can form if these transformations aren't controlled [42].

During rapid cooling, the carbon remains in solid solution. The austenite transforms to martensite: a body-centered tetragonal (BCT) crystal structure with a larger unit cell volume than the typical BCC unit cell of pure Fe iron that can accommodate the carbon atoms. The tetragonality of the structure is higher for higher carbon contents [35,42]. This change in crystal structure results in a volume increase – for a free body of 0.5 wt% carbon steel, this can be about 5 % [13]. Consequently, in components where only parts transform to martensite, residual stresses are induced in both the martensite (compressive) and the surrounding material (tensile).

Martensite has very high strength and hardness; however, it is very brittle. In railway operations, as discussed in Section 3, such hardened regions can break off from the wheel or rail surface – this is called "spalling". Reheating the material results in tempering of the martensite, allowing for the carbon in solid solution to segregate and for carbides to precipitate – this new microstructure has a lower density than martensite. This *tempered martensite* is a two-phase microstructure of ferrite and dispersed carbide which results in changes in the mechanical properties of the affected material, such as improved ductility

and toughness, and somewhat reduced hardness [35,43,44]. The tempering of martensite is seen in **Paper V**.

2.2.3. Phase transformations upon heating of pearlitic steel

From the binary Fe-C phase diagram, it is known that when carbon steel is heated to above the eutectoid temperature A_1, the microstructure transforms to austenite – this is typically given as (about) 727 °C [37]. When a hypo-eutectoid steel (<0.77 wt% C) is slowly heated to temperatures above the eutectoid temperature A_1, pearlite is transformed to austenite; while the free ferrite gradually transforms into austenite as the temperature increases up to the complete ferrite transformation temperature (the A_3 temperature). Some pro-eutectoid ferrite formed during production may remain unaffected or only partly transformed when temperatures are not high enough for complete austenitisation – this typically occurs when the temperature exceeds A_1 but remains below A_3. Extended exposure to temperatures above A_3 allows the ferrite to fully transform into austenite and carbon diffusion to lead to a homogeneous austenite with C in solid solution. In practice, the transformation temperature and transformation rate depend on the morphology and carbon content of the material, as well as the heating rate it is exposed to. As the heating rate increases, the transformation temperatures shift upwards – for this thesis work, this is referred to as the *effective* A_1 and A_3. Upon cooling, austenite transforms to ferrite, pearlite, bainite or martensite, depending on the cooling rate. **Papers IV** and **V** investigate cases of rapid heating and cooling yielding a martensitic structure as described in Section 2.2.2.

2.3. Mechanical behaviour

2.3.1. Mechanical properties

The tensile strength of pearlitic steel is highly dependent on the concentration of carbon and manganese. The carbon content dictates the amount of lamellar pearlite that can form, which allows for dispersion strengthening [37] . The addition of manganese shifts the eutectoid composition to lower carbon content (i.e. increasing the amount of pearlite formed at hypo-eutectoid carbon-content), and it acts as a solid solution strengthener and grain refiner. As mentioned in Section 2.2.1, the strength of pearlite is also affected by the interlamellar spacing – a finer microstructure results in higher strength. This could be attributed to the strain hardenability of pearlite via dislocations in the ferrite lamellae [37,41,45]. The carbon content should be optimised for strength, ductility and toughness. An increase in carbon, and thus in pearlite volume fraction, results in an increase in the impact transition temperature [37].

The room temperature micro hardness of cementite is about 1000 HV [46,47], while for ferrite it is in the range of 145 HV [48]. The hardness of pearlitic steel is dependent on the carbon content and interlamellar spacing – for the same carbon content, a finer pearlitic structure will have higher hardness.

For ER7T, the room temperature hardness of the web material is about 200 HV compared to about 280 HV in the rim (refer to the hardness map in Figure 4(a) of **Paper III**). R260 rail steel typically has a Brinell hardness between 260 and 300 [30] – the virgin hardness was measured for samples used in this study, and was found to be about 290 HV.

Microstructural changes, such as spheroidisation of pearlite or the formation of martensite (as discussed in Section 2.2) result in changes in the mechanical properties of the material. Increased spheroidisation in material intended for applications requiring high strength is detrimental – an increase in spheroidite results in a decrease in strength and hardness, as these properties depend on the presence of the lamellar structure. At the same time ductility and toughness will increase with more pronounced spheroidisation. Martensite formation on the other hand will result in increased strength and hardness; however, the microstructure is brittle, providing poor resistance to impact.

2.3.2. Strain aging and dynamic strain aging

The small amount of interstitial carbon and nitrogen present in iron is responsible for the yield point phenomenon during room temperature tensile testing of iron and by extension, in steel [32]. After the lower yield limit is reached, a horisontal (or flat) region is often observed – this is called the Lüders elongation [49–51] and can be characterised as localised plastic deformation. After this elastoplastic transition, generalised work hardening starts, and the stress-strain curve takes on the characteristic upwards slope. An interruption during the Lüders extension, where the material rests at room temperature for an extended time, can lead to diffusion of the interstitial atoms to dislocation sites. This diffusion process can be expedited by increasing the hold temperature to between 80 °C and 200 °C [32,52]. The diffused interstitials pin the dislocations again, resulting in a new yield point on reloading – this phenomenon is referred to as *strain aging*.

An increase in testing temperature results in an increase in the carbon diffusion rate. The interstitial atom diffusion and deformation occurs simultaneously, resulting in the primary yield point being replaced by multiple localised yield points in the material structure. This phenomenon is known as *dynamic strain aging* (DSA) and is characterised by a serrated appearance of the stress-strain curve [32,53,54]. It is often also referred to as *blue brittleness*, as it coincides with the temperatures at which an oxide with a blue interference colour is formed on the steel surface [32]. Testing under DSA conditions can result in decreased material ductility because of the increased dislocation density and carbide nucleation. For the studied railway steels, DSA occurs between approximately 200 °C and 300 °C, depending on the applied strain conditions [55].

2.3.3. Fatigue behaviour

Fatigue can be defined as the gradual development and growth of cracks in the material structure when it is subjected to repetitive (or cyclic) loading below the ultimate tensile strength of the material. In most steels the effect of fatigue is a permanent localised change that eventually leads to degradation of the mechanical properties, cracking and ultimately to failure [56,57]. Fatigue loading can generally be characterised as either high-cycle fatigue (HCF), low-cycle fatigue (LCF) or thermal fatigue, and materials need to be tailored for the specific operating conditions [56]. Previous studies have investigated the LCF behaviour of railway materials [58–60] – here the load cycling is characterised by a relatively low number of cycles with a substantial amount of plastic deformation.

Thermal fatigue is also a common phenomenon in railway operations such as block braking. In this case the cyclic stress is caused by heating and cooling cycles which result in repeated thermal expansion and contraction [56].

Ratcheting is a special fatigue case where plastic deformation accumulates under the application of an asymmetric cyclic stress [61–63]; i.e. under the application of a cyclic loading with a small non-zero mean stress. This is a common phenomenon that results in surface crack formation under rolling contact fatigue and has been studied on both rails and railway wheels [64,65].

2.3.4. Cyclic thermo-mechanical behaviour

In practice, different failure mechanisms can occur simultaneously, resulting in a unique fatigue behaviour. An example of this is thermo-mechanical fatigue (TMF), where mechanical and thermal cycling is combined either in-phase or out-of-phase [66–68]. Combined loadings can result in significant variation in the material response compared to that experienced during isothermal loading. A further complication is the addition of oxidation or creep which amplifies the damage incurred during thermo-mechanical loading.

Both railway wheel and rail material experiences thermo-mechanical loading during operation and maintenance. Although this research topic is gaining traction in the railway research community [69,70], the complex nature of the material behaviour and microstructural changes during thermo-mechanical loading needs to be better understood. In **Paper I** the effect of thermo-mechanical loading is investigated on railway wheel steel, where the early cyclic plasticity is investigated (focussing only on the first few cycles) during out-of-phase thermo-mechanical cycling. In this case, possible surface oxidation is not considered to affect crack growth.

RAILWAY OPERATIONS AND MAINTENANCE

3.1. Rails and railway wheels

The key sections of the rail and wheelset, as referred to in this thesis, are shown in Figure 4.

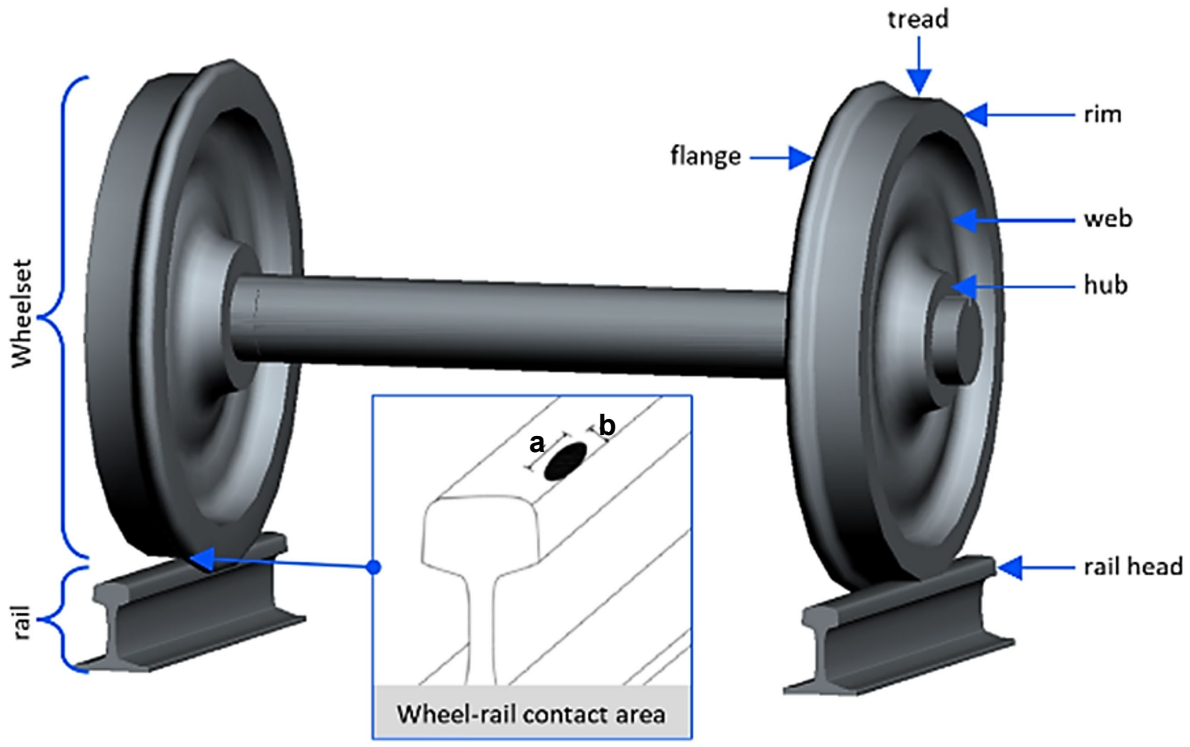

***Figure 4**: Components of a wheelset with a typical S-type wheel on a UIC 60E1 profile rail, identifying the wheel-rail contact area (from* [71] *under CC by 4.0 licence)*

3.1.1. Railway wheel design and production

Railway wheels should be designed for strength and good resistance to wear, while considering noise characteristics. However, different properties are required in different sections of the wheel as shown in Figure 4 [23,25,72]. The web must withstand the mechanical loads imposed by the rolling stock, while resisting fatigue and thermal stresses. This can be achieved by varying web curvature and thickness. The rim, on the other hand, is susceptible to tread wear and rolling contact fatigue (RCF), which is mitigated by increasing the rim hardness during production. Rim chilling is a heat treatment process whereby the entire wheel is heated to an austenitic microstructure (ca. 850 °C) and then the rim is cooled with agitated water to produce a hard, fine-pearlitic layer as shown in Figure 5. The inter-lamellar spacing (ISP) is approximately 125 nm and the free (pro-eutectoid) ferrite content is approximately 10 % at a depth of 20 mm below the tread surface of a new wheel. Both the pearlite ISP and the free ferrite content increase gradually with depth, leading to a slight reduction in hardness. In the web section close to the hub, the

ISP is approximately 250 nm and the free ferrite content is about 16 % [34,45]. The material for these rim-hardened wheels is designated with a *T* after the steel grade, e.g. ER7T.

***Figure 5**: Rim chilling facilities at Lucchini RS in Lovere, Italy*

3.1.2. Rail design and production

As discussed in Section 2.1, EN 13674 is used to standardise European rails. Vignole rails are covered in Parts 1 and 4: Part 1 for heavier rails (46 kg/m and above) and Part 4 for lighter rails (27 to 46 kg/m) [24,30]. Vignole rails, which make up the majority of rails in service, are symmetrical, flat-bottomed rails. Most European infrastructure managers use heavier rail profiles; 54E1 and 60E1 are the most commonly used. The 60E1 rail profile, as specified in EN 13674-1 [30], is shown in Figure 6. The rail profile is important, because it affects the wheel-rail interface and contact-area as shown in Figure 4. Improper contact between the wheel and the rail can result in damage to either component, leading to increased maintenance requirements, premature replacement or failures. Reprofiling should therefore be part of rail maintenance strategies.

Simultaneously, rail maintenance activities such as grinding or milling should be optimised to ensure that no significant microstructural changes occur. EN 13674 (clause 3) requires a full pearlitic microstructure; however, inappropriate machining can cause thermal damage to the surface layer of the rail, which can lead to undesirable microstructures such as martensite [30]. Typically rail material R260 has an ISP of around 230 nm in the top of the rail head [34,45]. The higher carbon content of R260

results in a fully pearlitic microstructure with similar hardness and strength to the ER7T wheel steel, despite the larger interlamellar spacing.

Premium, or head hardened, rails are heat treated during production to ensure a high hardening depth while keeping the hardness homogeneous over the cross-section and length of the rail [29].

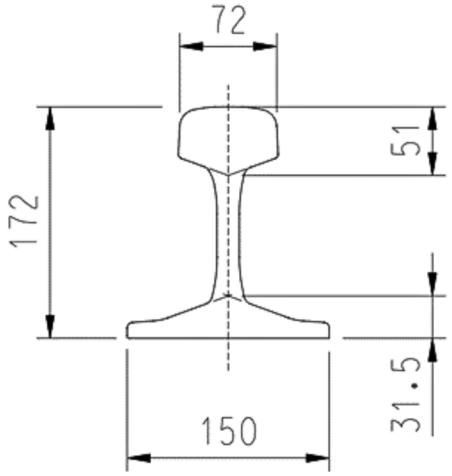

***Figure 6**: UIC 60E1 Vignole rail profile (units in mm)*

3.2. Railway operations and damage mechanisms

Rail deterioration is influenced by the type and amount of traffic, with a distinction made between passenger, freight, or mixed traffic on railways. The dynamic loads during operation also affect rail deterioration, which can be influenced by factors such as train weight, travel speed, and wheel-rail contact [73].

The shape of the contact area, as shown in Figure 4, changes as the wheel and rail wear during operation. This can have detrimental effects due to changes in the contact loading [74,75]. The highest stresses on the wheel are in the flange and tread surface. Frictional forces in the wheel-rail contact area, combined with rolling contact fatigue, can cause wear and crack formation on both the wheel and rail surfaces. This is aggravated during block braking or traction, occasionally resulting in wheel sliding, material yielding, and undesirable phase transformations.

Atoms are rearranged during plastic deformation, causing high temperatures in the surface layers of the components. As the wheel slides along the rail, it is exposed to more heat for a longer time, reducing the temperature gradient. Depending on the temperature that is reached locally, pearlite will spheroidise or transform to austenite – the reduction in temperature gradient allows for greater volumes of the pearlite to be affected. When the wheel starts rolling again, the heat dissipates quickly, which can result in high cooling rates. At sufficiently high cooling rates, the newly austenitised regions in the surface layer will transform to martensite. These phase transformations in the wheel tread surface

(discussed in Section 2) can be detrimental to the mechanical properties and introduce residual stresses, increasing the risk of cracking or other surface damage [13,36,76–78].

Surface damage, such as plastic deformation, crack development and thermal damage, alters the profile geometries of the wheel and rail. This in turn changes the contact loads, which can induce vibrations that aggravate the dynamic loading and lead to more severe surface deterioration [15,75,79]. As a result, maintenance needs are increased.

3.3. Railway maintenance

High demands on railway traffic due to more frequent passenger transit services and increased freight transport, results in limited available railway maintenance windows. In **Paper VI** the current practices throughout Europe are evaluated: it is clear that railway maintenance is considered a priority; however, the maintenance strategies and techniques used vary significantly. In this study it was found that there is currently a lack of knowledge on how to optimise rail machining techniques; similarly, there are insufficient predictive tools to allow for effective planning the required maintenance.

Grinding and milling are the most common surfacing technologies used to remove surface damage and reprofile the wheel tread or rail head. This improves the wheel-rail contact. A wheel can typically be reprofiled two to five times during its lifetime, depending on the severity of the damage. Higher material removal is required for more severe damage, including subsurface cracks. Some preventive maintenance strategies, such as the scraping technique used on railway wheels by the Dutch railways [75], require frequent removal of a thin surface layer. Subtractive machining processes remove the damaged surface layer and expose new material with properties varying slightly from the original surface.

Additive repair techniques, such as repair welding, can be used to address localised damage and so eliminate the need for the replacement of entire rail sections. In rail repair welding, the damaged area is cut out and the head of the rail is rebuilt layer by layer. The excess weld deposits are then ground flush to restore the profile. It should be noted that welding is generally not permitted on railway wheels. However, there is ongoing research into methods of restoring the flange or tread to sufficient dimensions by overlay welding [80–82]. Rail repairs typically involve multi-pass fusion welding techniques. These include manual metal arc welding (MMA) and submerged arc welding (SAW) [75,82]. Rail welding techniques for joining rails, such as thermite or flash butt welding, have a high heat input. In contrast, rail repair welding has a low heat input and uses small weld beads, resulting in higher cooling rates. Each subsequent weld pass causes heat treatment of the previous weld deposit layer(s), gradually altering its material properties. This results in localised thermal loads, which provide necessary tempering for a more ductile behaviour; however, this can cause unwanted microstructural changes, such as local bainitic or martensitic regions, and mechanical property gradients [75,83].

Both subtractive and additive maintenance techniques require well defined procedures based on the actual material behaviour during different thermal processes. The material response to thermo-mechanical loads is similar during railway operations and maintenance; therefore, the findings from studies in either field can be used to establish universal principles.

RESEARCH METHODOLOGY

The work presented in this thesis was done to characterise the behaviour of railway wheel steel ER7T and rail steel R260, as discussed in Section 2. This section describes the testing, characterisation and analysis methods used in the investigation.

4.1. Samples

In **Paper I** the thermo-mechanical behaviour of the virgin wheel rim material was investigated during slow heating and controlled cooling. In **Paper II**, the effect of this thermo-mechanical loading on the microstructure of near-pearlitic steel was studied. For a comprehensive overview, the experimental series for this study was extended to include virgin wheel web material, which has somewhat different mechanical properties since it is not exposed to the rim chilling process (as described in Section 3.1.1). Six experimental series were executed and subsequently used to calibrate a material model for severe block braking developed in **Paper III**. This thermo-mechanical testing was performed on cylindrical test bars supplied by Lucchini RS, taken from the locations shown in Figure 7(a), with typical test bar dimensions shown in Figure 7(b).

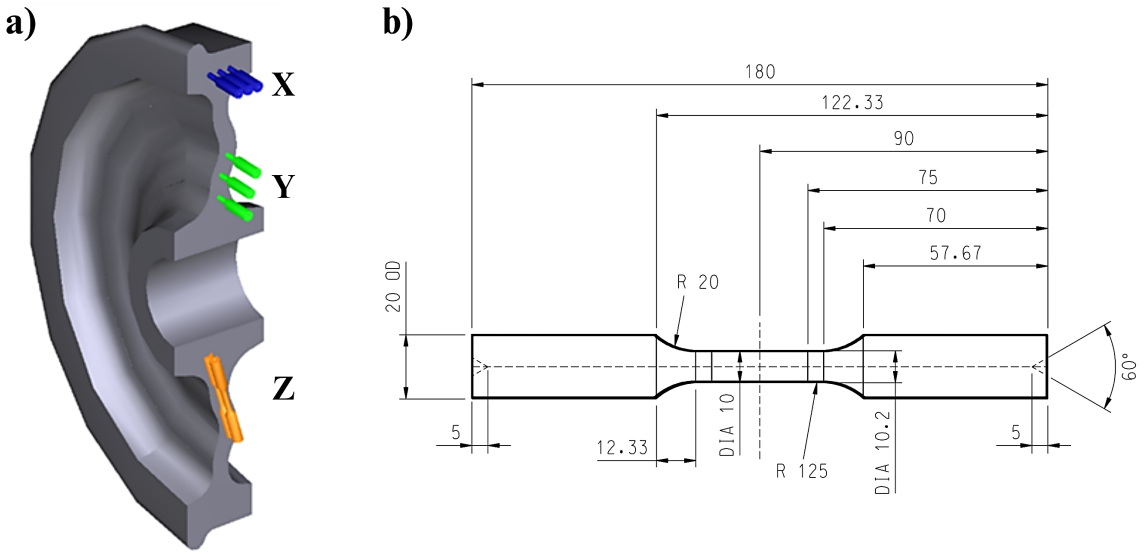

***Figure 7**: **a)** TMF sample locations on virgin ER7T railway wheel. Distinction is made between rim samples (X), circumferential web samples (Y) and radial web samples (Z). **(b)** Standard test bar geometry as used for Papers I, II and III*

The effect of rapid heating and cooling on wheel rim material was studied in **Paper IV** using samples taken from the wheel rim, as shown in Figure 8(a), with a diameter of 95 mm and thickness of 25 mm as shown in Figure 8(b). An unused ER7T railway wheel was supplied by Lucchini Sweden AB; these samples were machined from the wheel rim to be used as build plates in an EOS M100 metal printer (see Section 4.5 for more detail). The surface used for the study in **Paper IV** is from a depth of

approximately 30 mm below the wheel rim surface, at a plane parallel to the surface. This is a relevant depth since it becomes surface-near after a few reprofiling cycles. A small build plate with a diameter of 50 mm and a thickness of 20 mm, as shown in Figure 8(d), was cut from the head of a virgin rail section as shown in Figure 8(c) – the resulting exposed surface was about 5 mm below the nominal rail head surface. A custom sample holder was used to mount this build plate in the M100 metal printer.

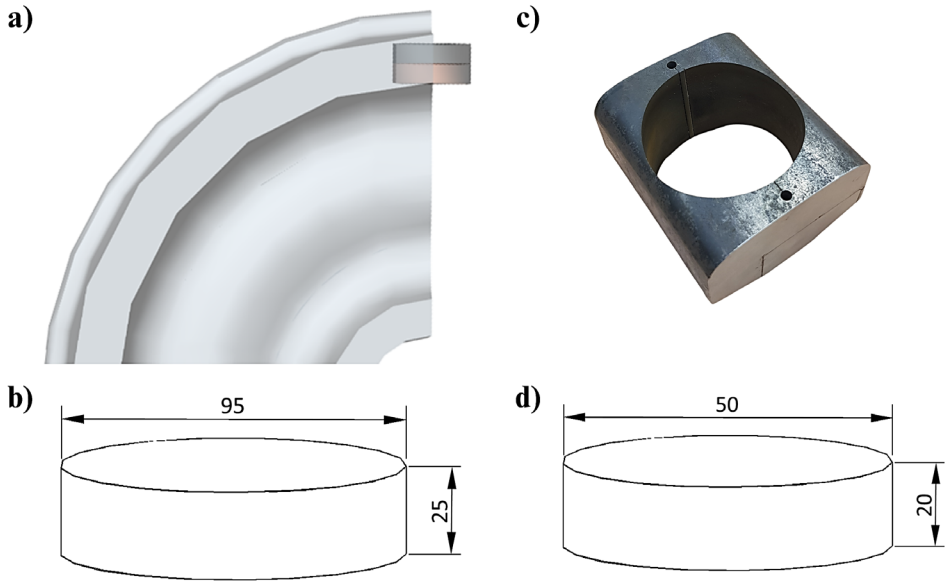

Figure 8: a) *Position where the build plates were taken from the wheel rim.* ***(b)*** *Machined size of each ER7T build plate* ***(c)*** *A small build plate was machined from the rail head – the diameter was limited by the semi-flat top surface of the virgin rail.* ***(d)*** *Machined size of the R260 build plate, which was then fitted to a sample holder to fit the M100 printer (see Section 4.5). All units in [mm].*

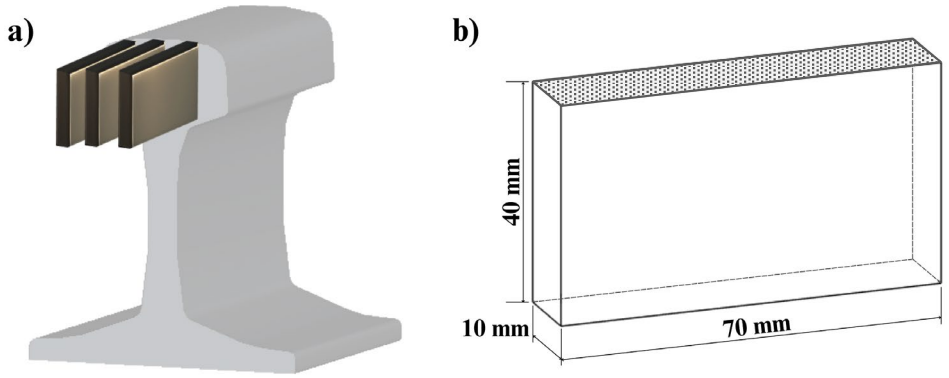

Figure 9*: Illustration of the samples for Paper V with* ***(a)*** *showing the position and orientation of the samples taken from the rail head and* ***(b)*** *sample dimensions.*

Rapid heating and cooling occur during rail machining processes, such as rail grinding. The effect of grinding on the rail head microstructure was studied in **Paper V**. Samples for grinding were taken from an unused rail head, from locations as shown in Figure 9(a) – each sample was machined according to the dimensions shown in Figure 9(b) with the top surface (indicated by the shaded region) left in the as-received condition. This would allow for grinding experiments to be performed on material similar to that of a new rail installed in field. The dimensions of these samples were chosen to ensure that there is

sufficient bulk material for self-cooling, in order to be representative of the rail machining performance in practice.

4.2. Thermo-mechanical testing

The thermo-mechanical testing, as described in **Paper I**, was used to experimentally simulate the effect of severe block braking on railway wheels – this paper investigated the effect of thermo-mechanical loading on the material behaviour, while **Paper II** investigated the effect on the microstructure of the material. **Paper III** describes how these results were used to calibrate a new numerical model for severe block braking, which aimed at further developing an existing isothermal numerical model to include thermo-mechanical effects.

4.2.1. Test setup

Thermo-mechanical testing was done using induction heating on an MTS 809 servo-hydraulic biaxial test frame fitted with a 100 kN load cell – for this study the torsional direction was locked and only axial loading channels were used. Figure 10(a) shows a photo of the setup. K-type thermocouples were welded onto the test bar in two places – one for control in the centre of the gauge section and the other as a safety measure on the radius of the lower grip section. The thermocouples were spot welded around at least half the circumference of the test bar, as shown in Figure 10(b). An MTS water-cooled high-temperature extensometer fitted with ceramic extension rods were used to measure the strain.

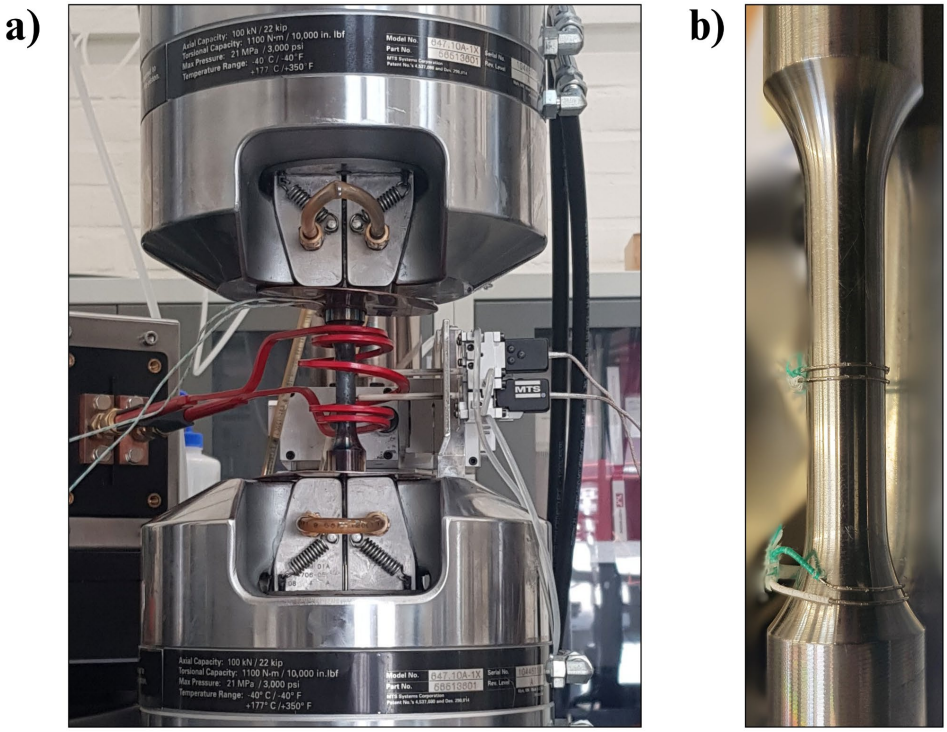

Figure 10: ***(a)*** *Experimental setup in the MTS 809 machine with the induction coil and high-temperature extensometer installed.* ***(b)*** *K-type thermocouples spot welded around half the circumference of the test bar.*

4.2.2. Procedure

The strain-controlled thermomechanical testing was done according to the TMF code-of-practice [84]. The testing procedure, as outlined in Figure 11, is described below.

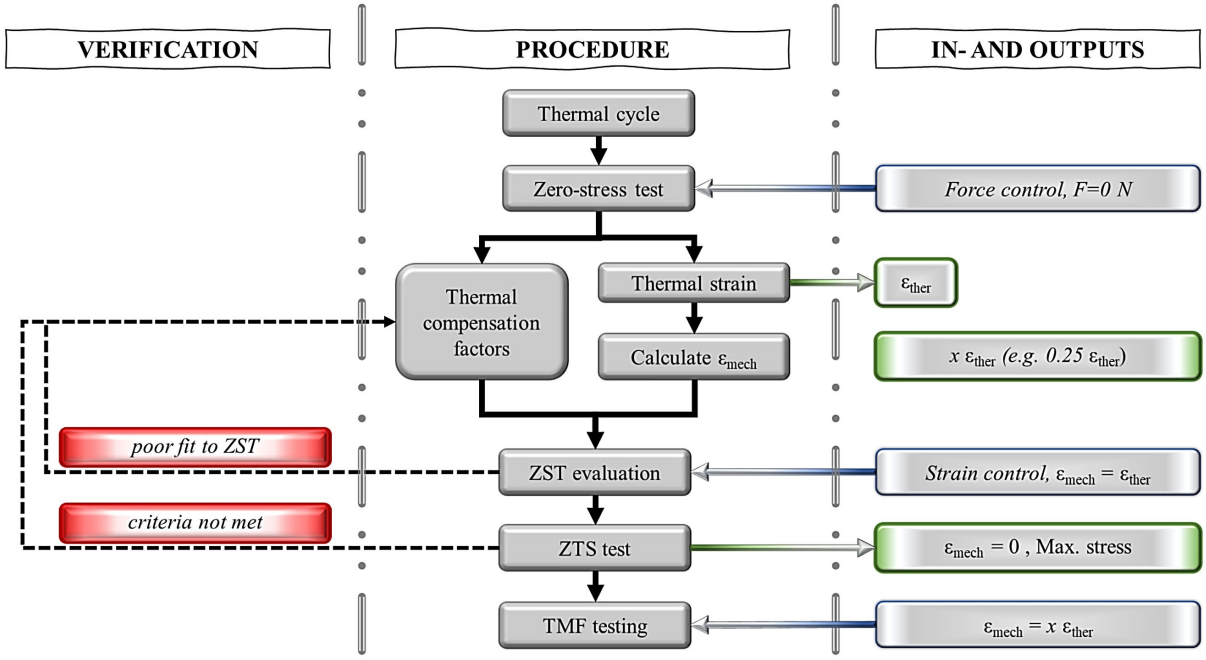

***Figure 11**: Outline of the procedure used for TMF testing, with user controls and variables to the right, and verification loops to the left.*

Application and thermal cycle

The numerical model for severe block braking developed in **Paper III** used a thermal cycle with a peak temperature of 650 °C as the initial case, based on field study measurements and previous models for tread braking [85–88]. However, this would allow for the worst-case scenario. Typically, the rim material would seldomly be exposed to peak temperatures above 600 °C, while the peak for the web material is expected to be 300 °C at maximum.

To allow for the scaling of the initial thermal cycle to other peak temperatures, two exponential functions were used to describe the heating and cooling curves respectively:

$$T_H = -700ke^{-0{,}00098x} + 700k$$
$$T_C = 3300ke^{-0{,}00056x} - 40k$$

with T_H the temperatures on the heating curve, T_C the temperatures for the cooling curve, x the time (in seconds) and the scaling factor, k, a factor describing the peak temperature relative to 650 °C, i.e.:

$$k = \frac{T_1}{650}$$

Initial testing of the rim samples was done with a baseline, or minimum, temperature of 30 °C. However, due to fluctuations in ambient conditions and instability of the induction heating at such low temperatures, this was increased to 50 °C. The simulated braking cycle was 45 minutes long, as in the

field study [85–88]; therefore, the duration of the heating cycle was kept constant at 45 minutes for all peak temperatures. The cooling cycle was approximately 60 minutes, with slight variations to allow for the material to reach the baseline temperature according to the equations above. The different evaluated thermal cycles are shown in Figure 12.

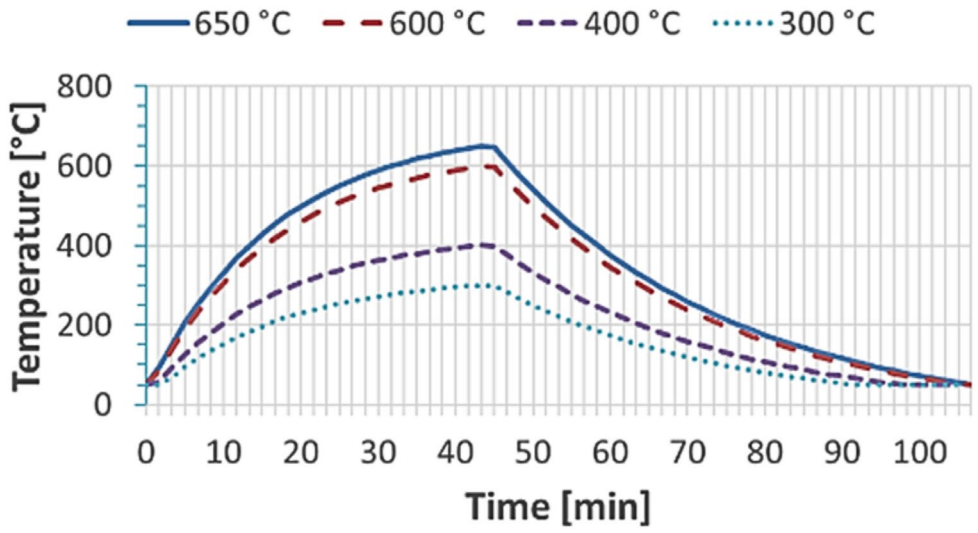

***Figure 12**: Evaluated temperature curves at different peak temperatures, with a 45-minute heating cycle and cooling for ca. 60 minutes.*

Zero-stress test

The testing procedure starts with a zero-stress test (ZST) under force control, where the sample is subjected to the programmed thermal cycle while free expansion is allowed. During this test, the amount of thermal expansion, i.e. the thermal strain, is measured. Five thermal cycles are executed to allow for stabilisation of the material, after which another five evaluation cycles are recorded to use for subsequent calculations.

Thermal compensation and calibration

During the zero-stress test (ZST), the measured total strain would be equal to the thermal strain. When mechanical strain (induced by force application) is applied, the total strain becomes the sum of the mechanical and thermal strains. In this study, mechanical strain and temperature variation was defined, and strain-controlled testing was done. To evaluate the mechanical strain separately, the thermal strain needs to be removed from the total measured strain through thermal compensation (see Figure 13). Curve fitting of the thermal strain measured during the zero-stress test is used to calculate initial thermal compensation factors E_2, E_1 and E_0. For this study it was found that a polynomial fit provided the most accurate results. The thermal strain is calculated at every time step from the temperature measured at the centre of the gauge section using the following formula:

$$\varepsilon_{th} = \boldsymbol{E_2}T^2 + \boldsymbol{E_1}T + \boldsymbol{E_0}$$

Thermal compensation is a programmed function of the MTS testing software where the thermal strain is calculated, then subtracted from the total measured strain. The compensation factors E_2, E_1 and E_0 are

then refined for the specific test series through an iterative experimental process (see the validation process in Figure 11). The zero-stress test is evaluated under strain control by programming the thermal strain measured during the ZST and verifying that the programmed thermal compensation results in near-zero stress throughout the test. Following the guidelines of the TMF code-of-practice [84], the thermal compensation factors were considered sufficient if the following criteria were met during the evaluation run:

- Peak stress values should be lower than 0.05 x $\Delta\sigma$ (full stress range of the TMF test)
- Mean stress should be lower than 0.02 x $\Delta\sigma$ (full stress range of the TMF test)

Determining strain values and TMF testing

As discussed in **Paper III**, the simulated use-case accounted for mechanical strains between 30 % and 60 % of the thermal strain at different positions in the wheel. The applied mechanical strains (now the total measured strain after compensation) should therefore be calculated as percentages of the measured thermal strains.

To cover the entire spectrum, five degrees of thermal dilatation restriction were investigated in this study:

a. Free expansion. Mechanical strain, thus the degree of thermal dilatation restriction, is zero.

b. 25 % thermal dilatation restriction

c. 50 % thermal dilatation restriction

d. 75 % thermal dilatation restriction

e. Full restriction. Mechanical strain is equal to 100 % of the calculated thermal strain, and thermal dilatation is fully restricted.

Figure 13 is a visual representation of the process. During the zero-stress test (ZST), full expansion is allowed; the machine controller is set to maintain zero axial force and the strain measured is thus only due to thermal expansion. Thermal compensation is then tuned to remove the effect of thermal expansion (i.e., thermal strain). With thermal strain removed by the software, the total strain is equal to the applied mechanical strain:

$$\varepsilon_{total} = \cancel{\varepsilon_{thermal}} + \varepsilon_{mechanical}$$

To get a zero-stress case (full expansion) even if we run the test under strain control, we need to allow for the thermal expansion by applying a mechanical strain. As an example, case **a** in Figure 13 shows how free expansion is simulated by applying mechanical strain equal to 100 % of the thermal strain as measured during the ZST. In essence, this is a test of how well the thermal compensation works, and the smaller the stress levels registered, the better. Cases **b** to **d** show different degrees of restriction of the

thermal dilatation and case **e** shows full restriction where the total strain is set to zero. Five thermal cycles were performed for each strain case at each peak temperature. Four test series were conducted on the wheel rim material at peak temperatures of 300, 400, 600 and 650 °C respectively. Test series were also completed for both the circumferential and radial web samples (as described in Section 4.1) at a peak temperature of 300 °C, and for the circumferential web samples at 650 °C for use in **Papers II** and **III**. These temperatures correspond to a worst-case scenario in operation.

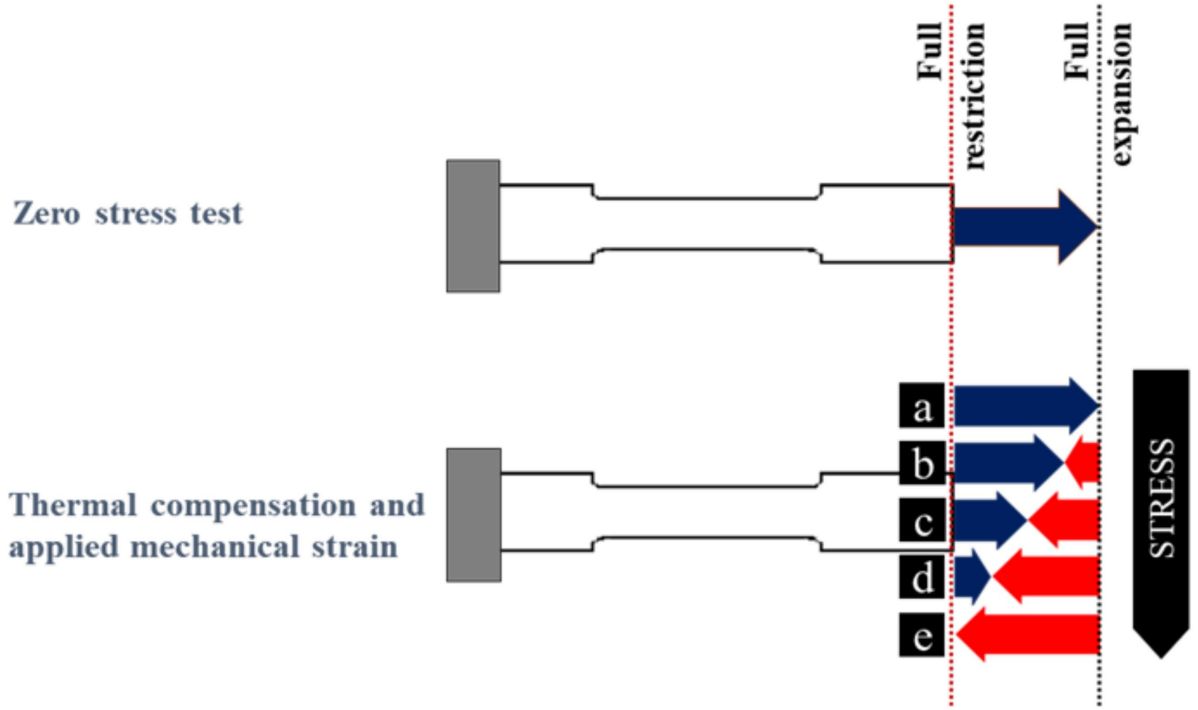

***Figure 13**: Thermal compensation and strain application during thermo-mechanical testing.*

4.3. Isothermal ratchetting

Previous studies have investigated the effect of isothermal testing between room temperature and 600 °C [34,89,90] – these strain-controlled experiments included investigation into the effect of hold times on the material behaviour. For complete calibration of the softening of the material during thermo-mechanical loading in **Paper III**, supplementary isothermal ratcheting tests were performed.

Testing was performed in the MTS 809 test rig with the same setup as described in Section 4.2.1 and shown in Figure 10. For the isothermal ratcheting tests (designated as rapidly heated tests in **Paper III**), the samples were heated to peak temperatures of 400 °C and 600 °C respectively – the peak temperature was reached within three minutes (180 seconds) and no additional hold times were used. This allowed for testing of material in a near-virgin state. Force-controlled testing was done with a zero mean-stress and only the first 10 cycles were considered for calibration of the softening behaviour in the numerical model for severe block braking.

4.4. Heat treatment

Previous studies on pearlitic railway wheel steel have shown that variation in mechanical properties, specifically room temperature hardness, can be expected after exposure to temperatures exceeding 500 °C [13,15,74]. To confirm that the hardness variation observed after TMF experiments with a low peak temperature of 300 °C (as done in **Papers I** to **III**) was a result of the combined thermal and mechanical loads rather than the elevated temperature alone, heat treatment was performed on virgin ER7T samples. A ceramic tube furnace with an argon atmosphere was used for the heat treatment at 300 °C and higher, and a laboratory oven was used for heat treatment at lower temperatures. All samples were allowed to air-cool. The following heat treatment was done on both ER7T rim and web samples (12 samples in total):

- 200 °C for four hours
- 250 °C for four hours
- 300 °C for 30 minutes and four hours (one sample each)
- 350 °C for 30 minutes and four hours (one sample each)

As noted in Chapter 4, the assumption is that railway wheel and rail material have a similar material response to thermo-mechanical loads. In order to understand the effect of elevated temperatures varied over time, additional heat treatment experiments were performed. A total of 50 cubic samples were heat treated – 25 ER7T rim samples and 25 R260 rail samples. The heat treatment was done using a ceramic tube furnace with an argon atmosphere at 300, 400, 500, 600 and 700 °C respectively. For each temperature, different samples were held for 5 minutes, 30 minutes, 105 minutes, 3 hours and 4 hours.

4.5. Laser scanning

In **Paper IV** the effects of rapid heating and cooling on near pearlitic railway wheel steel is investigated. This is done through comparing the results of laser scanning using the laser sources in two types of equipment: laser-based powder bed fusion (PBF-LB) additive manufacturing equipment and laser welding equipment. An overview of the experiments is given below.

4.5.1. Weld simulation using PBF-LB equipment

The PBF-LB additive manufacturing (AM) technique uses focused laser to fuse metal powder to build up a component [91]. For the experiments discussed in **Paper IV**, no powder was added; instead, the effect of the laser scanning heating the bulk material was investigated. The aim was to simulate the conditions in the heat affected zone resulting from the heat input during rail maintenance.

An EOS M100 metal printer for PBF-LB additive manufacturing with an Yb-fibre laser and argon atmosphere was used in these experiments. The laser speed and power density distribution can be varied depending on the requirements: the melt pool size and stability is dependent on the laser scan speed, whilst the power density distribution affects the material temperature [91,92]. For **Paper IV**, an effective laser power of 170 W and beam diameter of 40 µm was used. A zig-zag pattern was used to simulate a *single* scan band with a width of 1.5 mm as shown in Figure 14(a). An alternative scanning pattern, seen as the *wide* scan in Figure 14(a), was investigated to identify the effect of scan length – in this case, 15 mm long scans were made in a similar zig-zag pattern, up to a total width of 1.5 mm (thus considered as long scans compared to the width). Two different hatch spacings (50 µm and 100 µm) were considered and single scans were compared to overlapping scans, as shown in Figure 14(b), to evaluate the tempering capacity of subsequent scans.

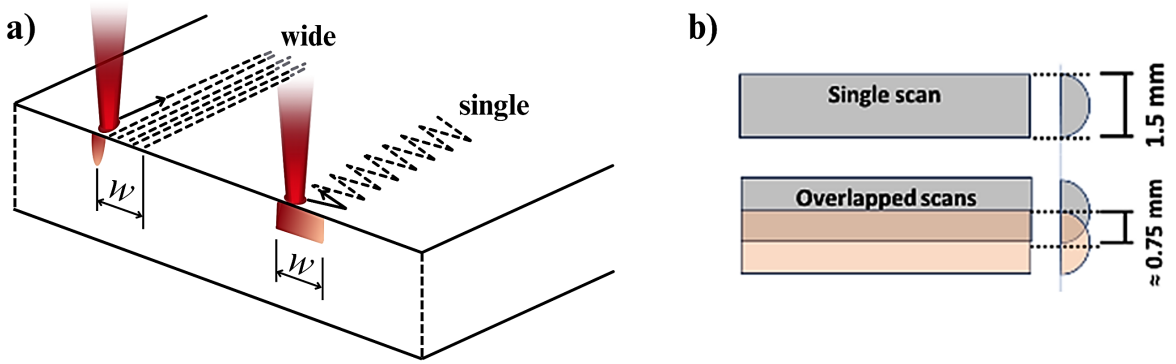

Figure 14: a) *Close-up illustration of the laser scanning showing the different scanning approaches for a single scan band (right) and a wide scan band (left), both with a width of w = 1.5 mm.* ***(b)*** *Scenarios to investigate the effect of subsequent scans*

4.5.2. Weld simulation using laser welding equipment

Heating by scanning with laser welding equipment was compared with the PBF-LB scans to understand how the variation in heat input from different process parameters can affect the material properties. AlphaLaser ALFlak900F laser welding equipment was used with a 2 mm diameter spot size, as shown in Figure 15, and argon shield gas. In the study presented in **Paper IV**, the scan speed and applied power was varied, and the resulting microstructural changes due to variation in heat input was investigated.

Three different laser forward scan speeds were considered to evaluate the effect of scan speed: 1.3 mm/s, 5.3 mm/s and 6.3 mm/s. Different scenarios were again investigated to study the tempering capacity of subsequent scans (as for the AM scanning).

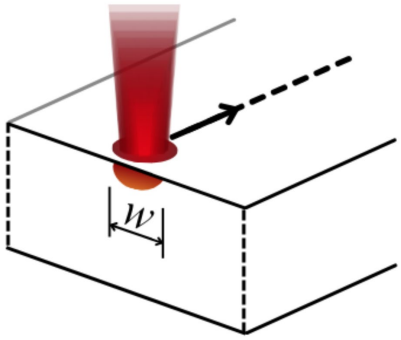

***Figure 15**: Illustration showing the approach for laser weld scans, with a width of about 2 mm.*

4.6. Hardness

Mounted samples were prepared by mechanical polishing down to 1 µm with diamond solution and finally active oxide (colloidal silica) polishing to 0.04 µm. Room temperature hardness testing was done using a Struers DuraScan-70 G5 hardness tester made by Emcotest. The hardness of virgin and TMF tested samples, as used for **Papers I, II** and **III**, was evaluated. At least ten random Vickers hardness (HV) indentations were made on each sample with a load of 30 kg and a hold time of 12 seconds. The hardness was measured for both gauge (tested) and grip (virgin) samples from each test bar; it was then normalised to the virgin hardness of the respective test bars. Additionally, a hardness map of the wheel profile was created for **Paper III**, using the same parameters.

To characterise the microstructural changes during rapid heating and cooling as discussed in **Papers IV**, Vickers hardness (HV) indents were made with a load of 1 kg and a hold time of 12 seconds across the top surface of each laser scanned band (as discussed in Section 4.5). Similar hardness testing was done to confirm the microstructure obtained during grinding, as discussed in **Paper V**.

4.7. Microscopy

Stereo optical microscopy was used for the surface evaluation of the scanned regions in **Paper IV**. A Zeiss Stereo Discovery V20 microscope with AxioVision V.4.7 software was used for this analysis. A 5 mm slice was cut from the build plate surface (see Figure 16) using electric discharge machining (EDM) to create cross-sections of the different scanned regions (as described in Section 4.5). The same metallographic preparation procedure as for the TMF samples (as described in Section 4.6) was used on all samples for microscopy and etching was done with 3 % nital (HNO_3 in ethanol).

The microstructure of the cross-sectional samples for **Papers IV** and **V** was investigated using a Zeiss Axioscope 7 light optical microscope with Zen Core 2.7 software. The microstructural analysis and subsequent spheroidisation quantification for **Papers I** and **II** required a higher magnification. Therefore, scanning electron microscopy was done using a LEO Gemini 450 field emission gun scanning electron microscope (FEGSEM). For the quantification of spheroidisation as described in **Paper II**, at least 70 images at a magnification of 5 000x were taken at random locations for each sample.

***Figure 16**: slice cut from build plate surface to prepare samples for microscopy*

4.8. Residual stress measurements

Residual stress measurements were done for the study presented in **Paper IV** using a Stresstech Xstress 3000 X-ray diffractometer with a type G2R tripod-mounted goniometer and a Cr Kα X-ray source. A 1 mm collimator was used and calibration was done on a pure ferrite (Fe) calibration block. Residual stress was measured on the top surface of each of the laser scans at inclination angles varying from -45° to 45° (in nine equal steps), each at three different rotation angles (0°, 45° and 90°). A Split Pearson VII fit was applied to the intensity distribution measures and the principal stresses were evaluated.

ANALYSES AND RESULTS

This chapter provides a summary of the analyses and results obtained from the individual studies as presented in **Papers I** to **VI**, as well as relevant unreported results.

5.1. Thermo-mechanical behaviour of railway wheel steel

A use case for severe block braking was simulated to explore the complex interaction of mechanical and thermal loads. The study in **Paper I** investigated the stress response of railway wheel steel ER7T under combined thermal and mechanical loading. Peak temperatures of 300, 400, 600 and 650 °C were considered, while the thermal dilatation was restricted at different degrees ranging from 0 % to 100 %, thus over the full spectrum of thermal expansion.

It was found that an increase in the degree of thermal dilatation restriction for a given peak temperature resulted in an increased peak stress and more plastic deformation was visible. Similarly, an increase in the peak temperature for a given degree of thermal dilatation restriction resulted in a larger residual tensile stress remaining in the material after cooling. However, it was seen that microstructural changes could counteract this stress development – as the peak temperature increases, an increase in spheroidised pearlite was noted, accompanied by a reduction in room temperature hardness. The evolution in microstructure is further discussed in Section 5.3.

A hypothesis for **Papers I** to **III** was that changes in mechanical properties occurs at lower temperatures for thermo-mechanical loading than for isothermal fatigue testing [34,74]. A particular property of interest is room temperature hardness. Figure 17 shows that a decrease in hardness was observed at peak temperatures exceeding 600 °C, as expected from isothermal test results. However, slight variations in the room temperature hardness can be noted for the tests with lower peak temperatures.

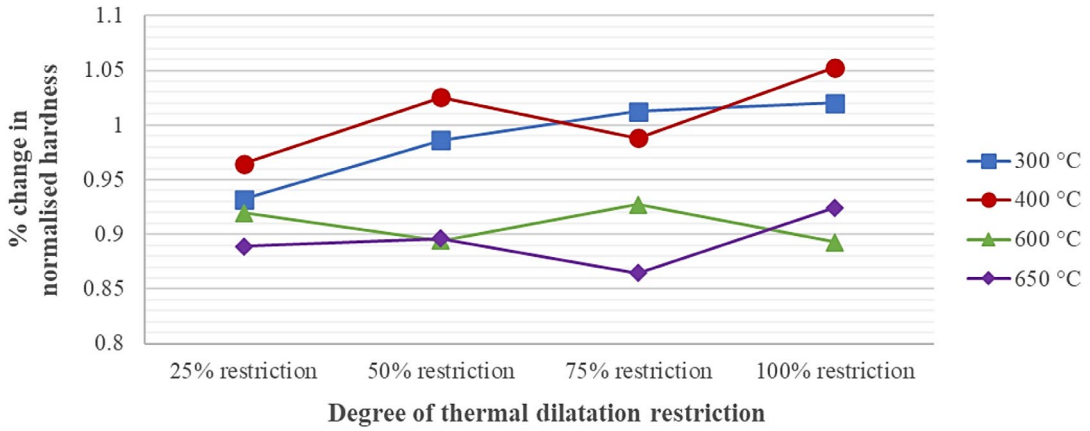

***Figure 17**: Variation in normalised room temperature hardness for railway wheel rim samples exposed to different peak temperatures and degrees of thermal dilatation restriction during thermo-mechanical cycling.*

Heat treatment experiments (as described in Section 4.4) were performed to determine if this variation is in fact due to the combined mechanical and thermal loads, rather than a result of the heat treatment alone. Table 2 shows the room temperature hardness values for the different heat treatment experiments (not included in appended papers) – it can be seen that heat treatment at temperatures below 400 °C does not affect the hardness of the material.

***Table 2**: Room temperature hardness of heat-treated samples*

	Room temperature hardness [HV30]			
	Rim material		Web material	
Virgin sample (min, max)	278, 286		189, 198	
Heat treatment	30 minutes	4 hours	30 minutes	4 hours
200 °C	-	282	-	198
250 °C	-	281	-	198
300 °C	282.5	282	194	193
350 °C	287	282	193	192

Paper III describes the development of a new constitutive material model for severe block braking. The experimental data from the thermo-mechanical testing, as discussed in **Papers I** and **II**, was used to calibrate this model. It captures the thermo-mechanical behaviour better than previous isothermally calibrated models and includes kinematic stress components to improve the fit to the plastic behaviour during thermo-mechanical cycling. This model also includes a softening law to predict microstructural changes at elevated temperatures, such as pearlite spheroidisation.

Supplementary isothermal ratcheting tests, as described in Section 4.3, were performed to provide data for the calibration of this softening law. Figure 18(a) shows the strain results for isothermal testing with a zero mean-stress at 400 °C for the first five minutes of the test; (b) shows the results for testing at 600 °C. Although the strain range is rather similar for the two tests, there is a clear accumulation of strain for the testing at 600 °C, i.e. a ratcheting response.

However, only the first ten cycles were of interest for the model calibration - Figure 18(c) and (d) shows the stress during the first minute of testing (about 14 cycles). The testing was performed under force-control, with the force kept constant throughout. The peak values were chosen to remain within the elastic region of the material based on material data from previous isothermal tests. Figure 18(e) and (f) were presented in **Paper III** to show the correspondence of the newly calibrated model to this experimental data. At 400 °C there is little deviation apart from the first cycle, which is expected since softening is not yet anticipated. At 600 °C softening will occur and as seen in (b) a ratcheting response is evident. There is a slight misalignment between the experimental and simulated results, which is expected at such a high temperature. Since the microstructure is very sensitive to changes in stress at

600 °C and given the asymmetric nature of the material response seen in the experimental data, exact fitting was not possible.

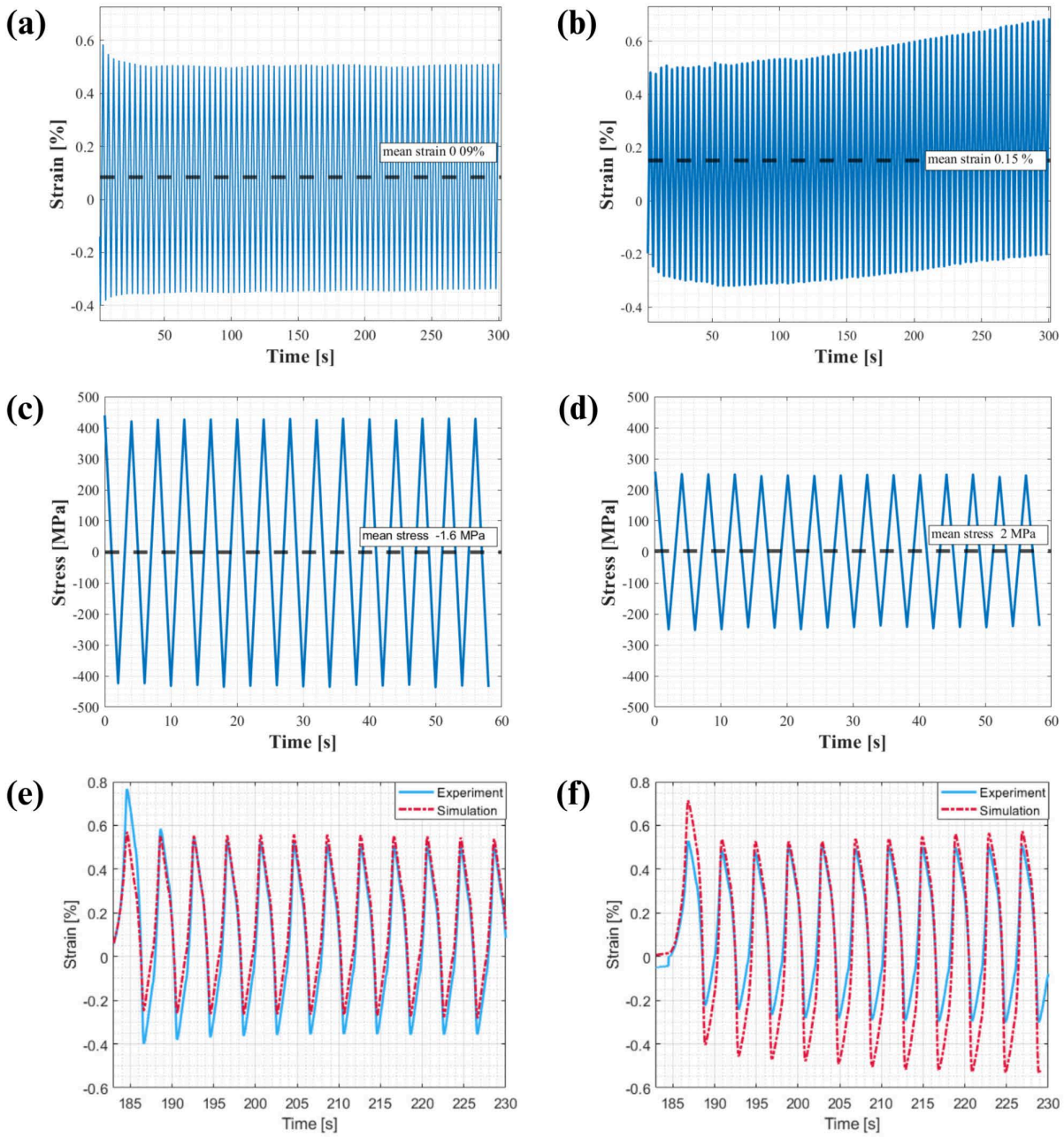

***Figure 18**: Results from isothermal ratcheting testing at 400 °C (left) and 600 °C (right) respectively. **(a)** and **(b)** shows the strain response for the first five minutes of cycling; **(c)** and **(d)** shows the applied stress with a near-zero mean; **(e)** and **(f)** shows the correlation between experimental and simulated results (plots created by E. Voortman Landström for Paper III)*

5.2. Effect of rapid heating and cooling on residual stress state

To contrast the slow heating and cooling cycles as investigated in **Papers I** to **III**, the effects of rapid heating and cooling was considered in **Papers IV** and **V**. The intent was to form a basis for subsequent studies into rapid, local heating events such as rail repair welding or grinding.

In **Paper IV**, the residual stress state was evaluated after laser scanning with different laser sources (see Section 4.5). Table 3 shows the scan parameters for each of the presented scans. Stress relieved samples were used as reference for the residual stress measurements. The study presented in **Paper IV** showed correlation between the material behaviour during scanning using the PBF-LB laser and scanning using the laser welding equipment. An increase in the forward scanning speed resulted in a decrease in the calculated surface energy density. However, it was determined that the applied power during scanning is the determining factor for the degree of surface heat absorption, which would determine the resulting material characteristics and residual stress field.

***Table 3**: Clarification of scan parameters used in Paper IV*

PBF-LB laser scan parameters					
Scan ID	**Scan format**	**Hatch spacing [µm]**	**Forward scan speed [mm/s]**	**Zig-zag scan width, *w* [mm]**	**Surface energy density[1], E_f [J/mm²]**
AM-1a	Single scan	50	6.3	1.5	17
AM-1b	Overlapped scans	50	6.3	1.5	17
AM-2a	Single scan	100	13.3	1.5	8.5
AM-2b	Overlapped scans	100	13.3	1.5	8.5
AM-3a	Wide scans	50	0.7	15	17
AM-3b	Wide scans	100	1.3	15	8.5
Laser welding scan parameters					
Scan ID	**Scan format**	**Applied power [W]**	**Scan speed [mm/s]**	**Surface energy density[1], E_f [J/mm²]**	
LW-1a	Single scan	900	5.3	85	
LW-1b	Two overlapped	900	5.3	85	
LW-1c	Multiple overlapped	900	5.3	85	
LW-2a	Single scan	450	1.3	173	
LW-2b	Single scan	900	1.3	346	
LW-2c	Two overlapped	900	1.3	346	
LW-2d	Single scan	600	1.3	231	
LW-3a	Single scan	600	6.3	48	
LW-3b	Two overlapped	600	6.3	48	

1. *Surface energy density calculations as described in Paper IV*

In this study, near-pearlitic railway wheel steel ER7T was compared to fully pearlitic rail steel R260. Although the behaviour and microstructure of the two materials are typically considered similar, it was shown that laser scanning resulted in more pronounced residual stress states in the fully pearlitic microstructure. This is attributed to the absence of pro-eutectoid ferrite in the R260, where the austenitised region transforms completely to martensite.

5.3. Microstructural evolution during thermo-mechanical loads

As described in Section 5.1, the thermo-mechanical behaviour of pearlite is investigated during slow heating and cooling in **Papers I** to **III**. **Paper II** focuses specifically on the spheroidisation of pearlite

because of these thermo-mechanical loads. Examples of micrographs extracted from the gauge section of several test bars used in these studies are shown in Figure 19.

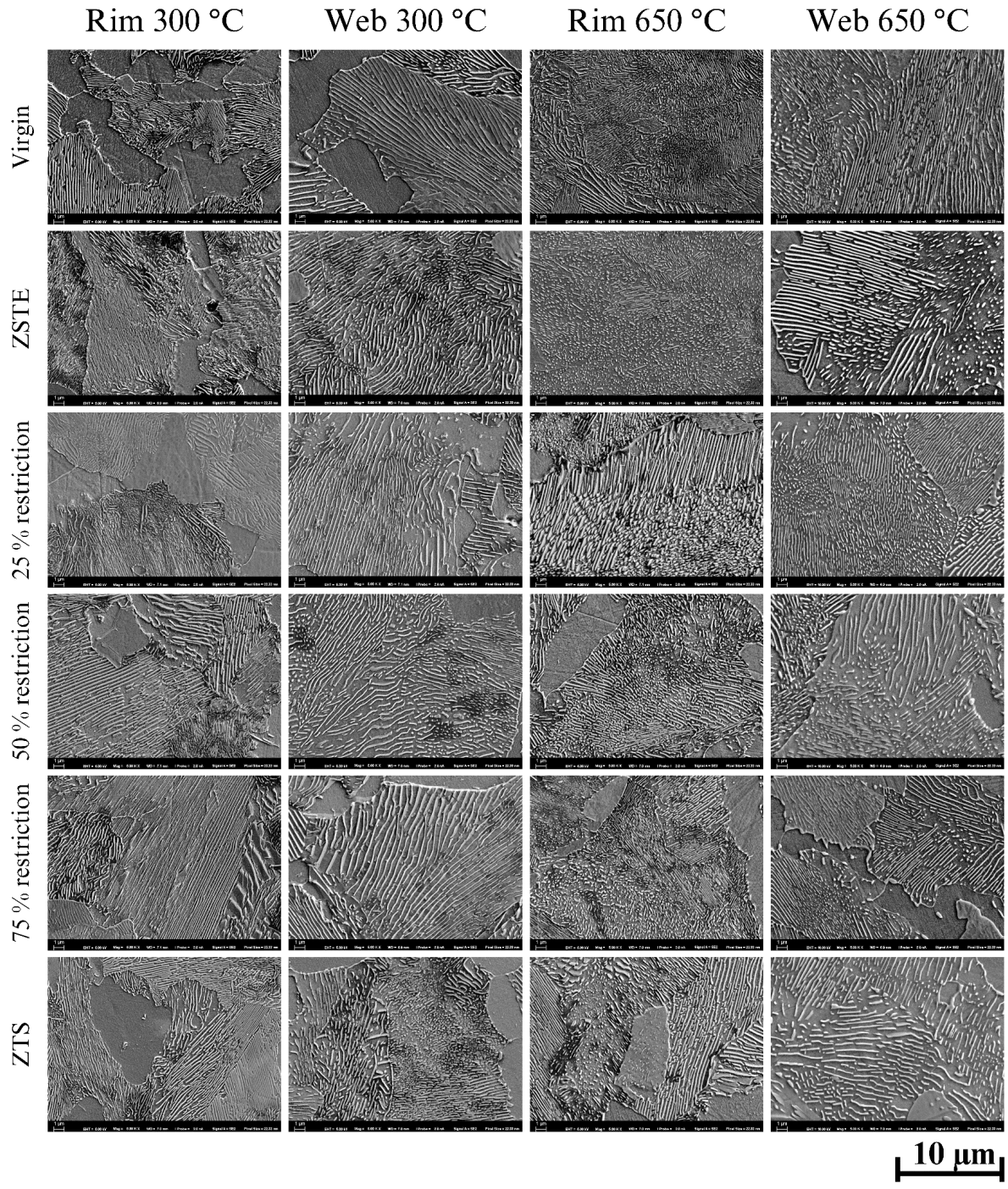

Figure 19: *SEM micrographs separated into different test series (by column). The top row shows the respective virgin samples, while the lower rows show the respective thermal dilatation restriction test results.*

Some spheroidisation is visible in the virgin samples as a result of heat treatment during the production process. After testing at 300 °C without restriction little or no change is visible in the degree of spheroidisation, while there is a high degree of spheroidisation for samples tested at a peak temperature of 650 °C. Although these observations are in accordance with previous studies [87,93,94], it is obvious

from the micrographs that quantification of the degree of spheroidisation is not possible solely on the analysis of the respective micrographs. It is therefore necessary to evaluate a larger region of the transformed material to gain a representative understanding of the extent of spheroidisation.

In this paper an image analysis method is proposed for the use of spheroidisation quantification. Each SEM image is analysed using Matlab – the amount of cementite present in the image is determined, and then the degree of spheroidisation is calculated as a fraction of the cementite volume fraction. Figure 20 shows the output from this analysis code, with the top half being the original SEM image and the bottom half showing the analysis output used for quantification.

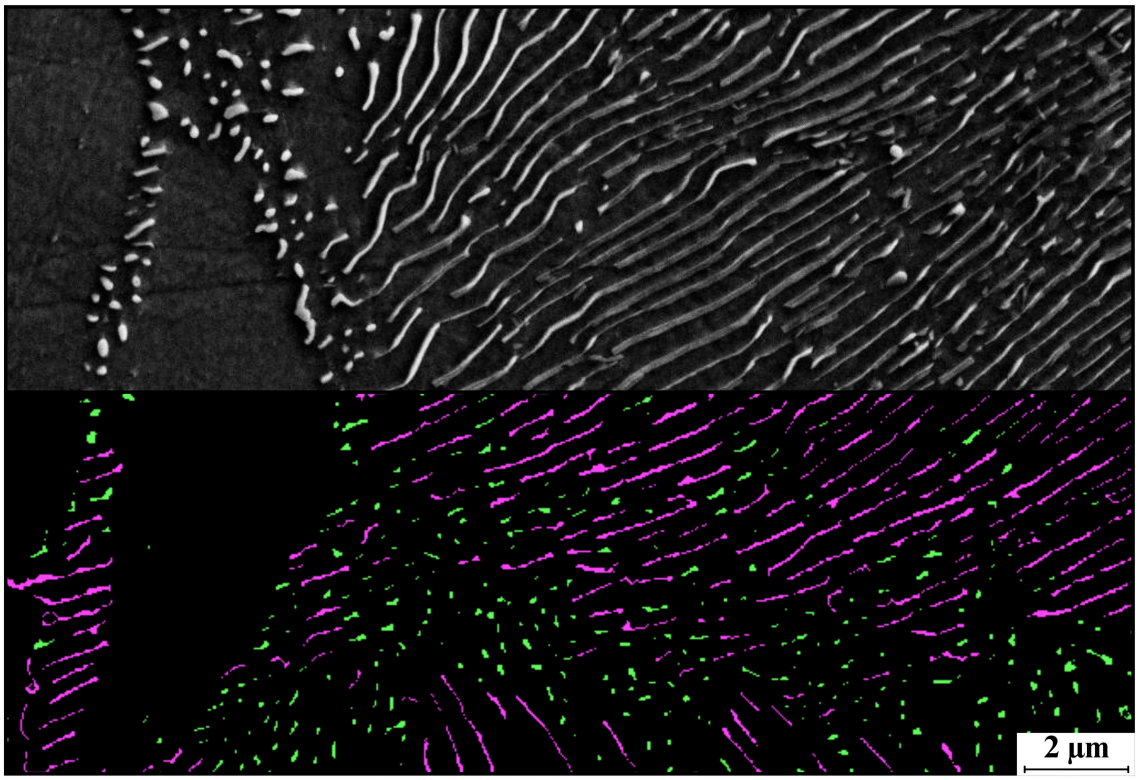

Figure 20*: Original SEM image (top) with the results from the image analysis overlapped at the bottom (shown on front page)*

The complementary statistics for the thermo-mechanical tests at 300 °C and 650 °C are considered. As expected, an increase in temperature results in an increase in the degree of spheroidisation. However, there is evidence that the degree of thermal dilatation restriction as well as the initial microstructure of the material will have an effect on the degree of spheroidisation. ER7T railway wheel material from the wheel rim and web is compared – the pearlite interlamellar spacing in the web is ca. 250 nm, compared to ca. 125 nm in the rim. The statistical findings in **Paper II** suggest that an increase in thermal dilatation restriction in the fine-pearlitic rim material will result in a decrease in spheroidisation at elevated temperatures, as shown in Figure 21.

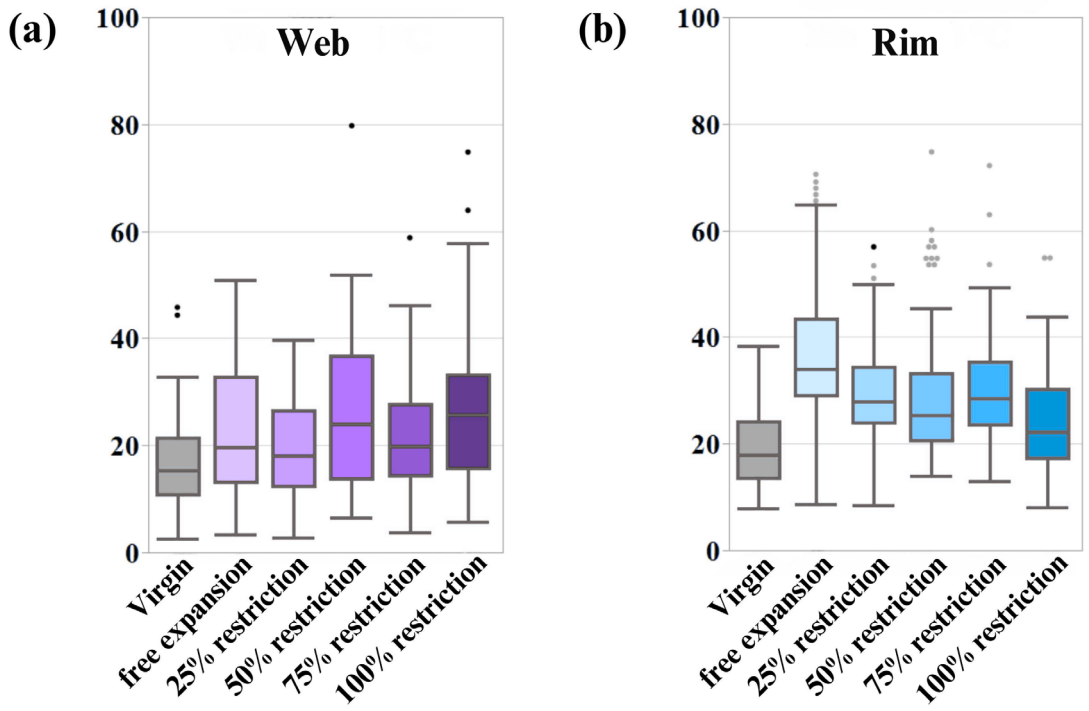

***Figure 21**: Box plots showing the spheroidisation quantification results for samples of railway wheel material ER7T exposed to thermo-mechanical cycling with a peak temperature of 650 °C. **(a)** Wheel web material with a pearlite interlamellar spacing of ca. 250 nm and **(b)** wheel rim material with a pearlite interlamellar spacing of ca. 125 nm*

Heat treatment (as described in Section 4.4) was performed to determine the influence of a pure thermal load. The solid lines in Figure 22 show the room temperature hardness values for the railway wheel rim material after the respective heat treatments. This shows that the material will in general soften when exposed to elevated temperatures and the results at the shorter hold times do not correspond with the findings as presented in **Paper II**. This supports the notion that the behaviour as discussed in this paper is a direct result of the restriction of thermal dilatation.

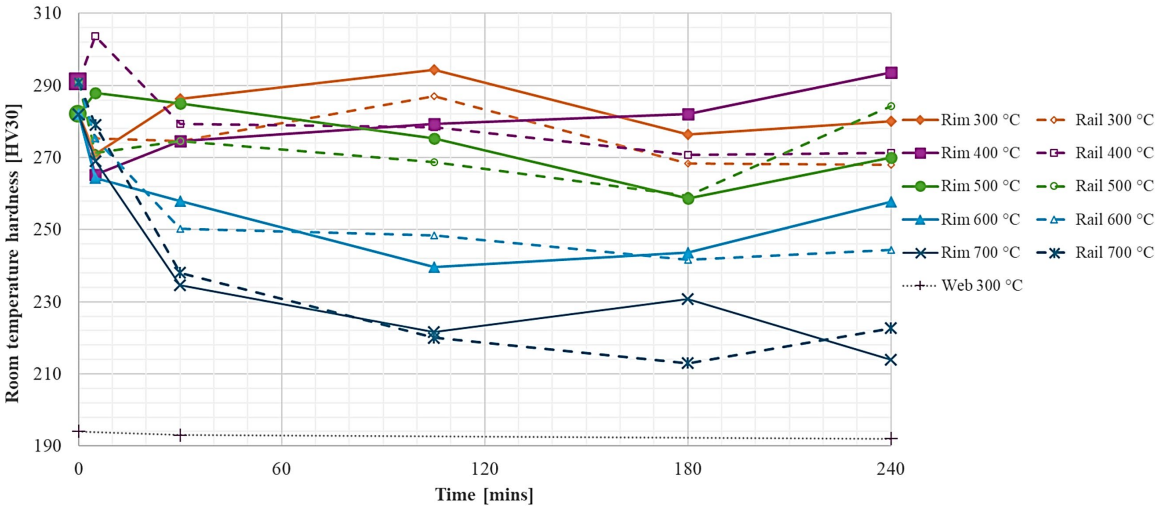

***Figure 22**: Room temperature hardness values for heat treated samples of ER7T railway wheel rim material (solid lines) compared to R260 rail material (dashed lines). Heat treatment was performed at temperatures ranging from 300 °C to 700 °C for 5 minutes, 30 minutes, 105 minutes, 3 hours and 4 hours respectively.*

An anomaly noted for the ER7T rim material is the apparent hardening after 4 hours for all temperatures up to 600 °C. The room temperature hardness measured for R260 rail material exposed to the same temperatures and hold times did not show this behaviour, as shown by the dashed lines in Figure 22. This indicates that it is a unique behaviour for the near-pearlitic ER7T steel.

Upon rapid cooling from temperatures above the austenitisation temperature, martensite will form. During rapid heating and cooling cycles, the thermal gradients are often very large, resulting in a localised transformation to martensite. This is investigated in **Papers IV** and **V**.

In **Paper IV** the effect of rapid heating and cooling is observed during heating by laser scanning using both additive manufacturing and laser welding equipment – examples of the transformed regions are shown in Figure 23. Similar to the residual stress results discussed in Section 5.2, correlation was shown between the microstructural changes resulting from the two processes for each material.

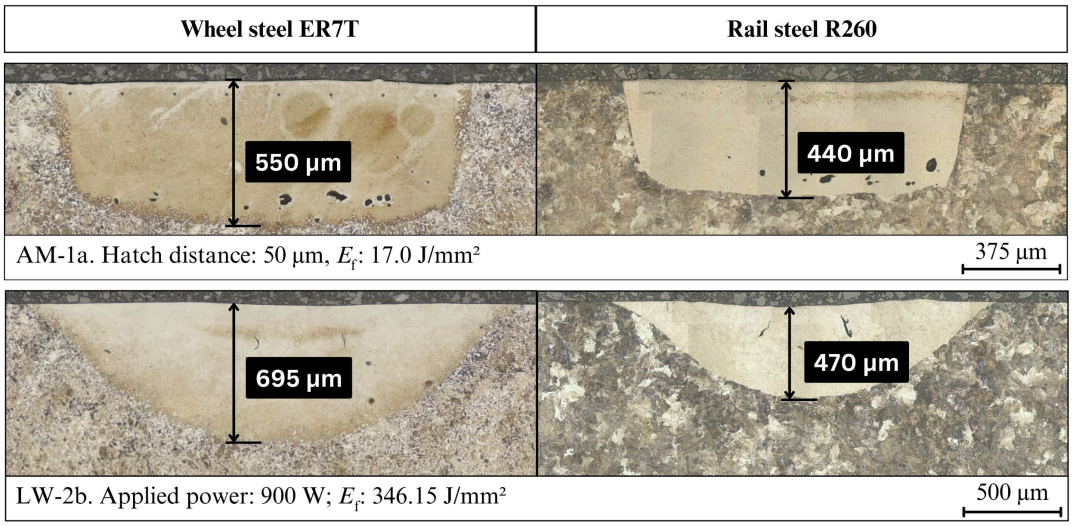

Figure 23: *Optical microscopy images of the transformed region created by laser scanning using additive manufacturing equipment (top) and laser welding equipment (bottom). The scan parameters can also be found in Table 3. The same scans were performed on both the near-pearlitic railway wheel steel ER7T (left) and the pearlitic rail steel R260 (right).*

The martensite formation during grinding operations are considered in **Paper V** – in this study, the effect of variation in process parameters were evaluated by considering the depth of martensitic transformation. Figure 24 shows the results from the grinding experiments on standard rail steel R260 compared to premium head hardened rail R350HT. As seen in **Paper IV**, the applied power (i.e. specific energy here) has a significant effect on the thickness of the martensite layer that formed.

Both spheroidisation and martensite formation result in altered mechanical properties and can influence the material performance in operation. These studies help to form an understanding of the effect of local heating processes on the microstructure – this can contribute to tailoring localised events during maintenance and operations to minimise the detrimental effects of these microstructures.

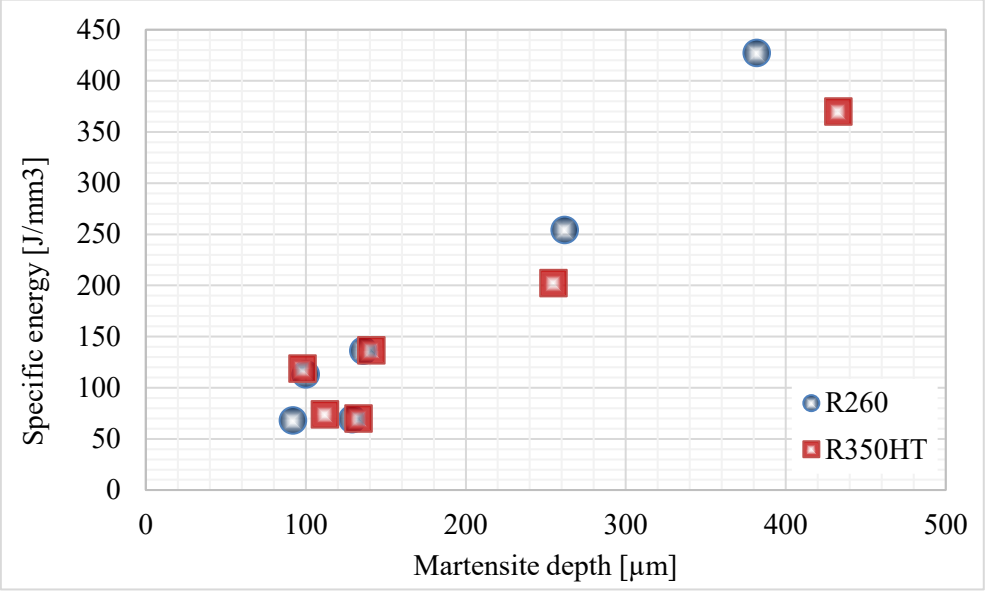

***Figure 24**: Correlation between the specific energy during laboratory grinding and the depth of martensitic transformation*

5.4. Practical applications

An ongoing theme throughout this thesis work was to find the relation between the fundamental material behaviour and characteristics, and the potential impact on real applications in practice. As discussed in Sections 3.2 and 3.3, the main applications for this thesis work focussed on railway operations and maintenance. As discussed in previous sections, **Papers I** to **III** investigated the thermal cycle from an actual operations use case of severe block braking. The experimental findings were linked to the practical case and to calibrate the improved constitutive material model for severe block braking.

Similar simulations to those used in **Paper IV** were used to simulate in-situ railhead repair welding in Paper A.1 (not appended to this thesis work). In this work a finite element method (FEM) based methodology was used to investigate the influence of welding process parameters on the quality of a repaired rail head. This included the evaluation of cyclic plasticity, phase transformations, transformation-induced plasticity and multi-phase homogenisation [95]. This shows that the knowledge can be transferable between different welding methods – in this case between manual metal arc (MMA) welding and laser welding.

However, a major challenge for the simulation of welding is the variation in resulting microstructures due to variations in the initial microstructure, weld filler material and the process parameters used. The micro-hardness and microstructures were analysed in the rail repair weld used for experimental calibration in Paper A.1. A summary of the hardness measurements is shown in Figure 25. Hardnesses of up to 350 HV1 is measured in the bulk of the material. However, in the regions built up from filler material and in boundary regions, larger variations occur. The resulting microstructures differ

significantly from the bulk pearlitic microstructure. Some of these variations are identified with letters in Figure 25 and shown in micrographs in Figure 26.

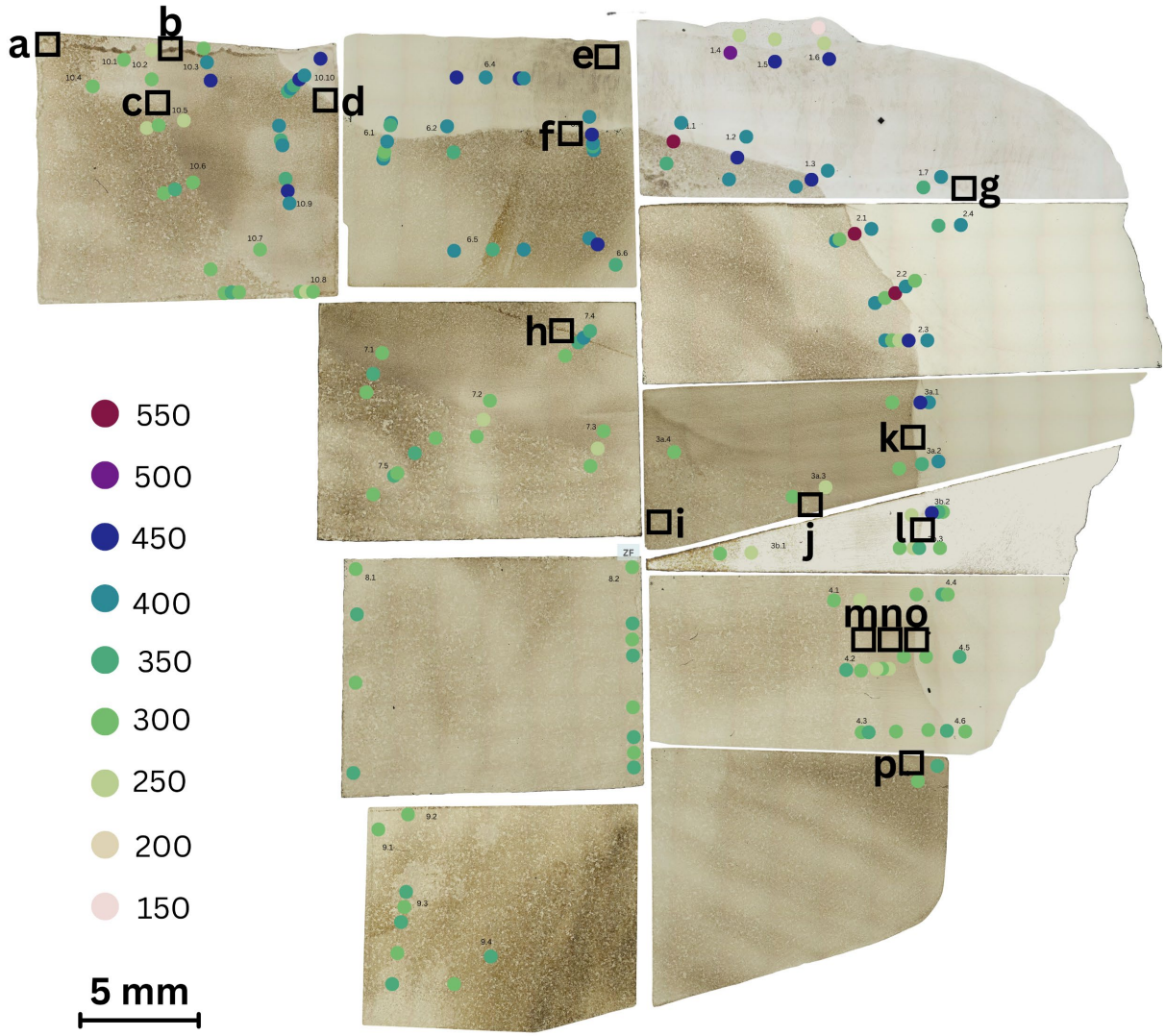

***Figure 25**: Summary of the micro-hardness measurements [HV1] taken across a rail head repair weld. Micrographs were taken of representative regions (marked with letters) – these results are shown in Figure 26.*

Although it is assumed that pearlite, bainite and martensite will form during the welding process (based on the simulated results). The microstructures presented in Figure 26 were not analysed, identified or characterised; however, the hardness measurements were used to verify the effects of predicted phase transformations.

Another field of particular interest for railway infrastructure managers is rail surfacing; specifically, railway grinding. **Paper IV** and **V** was intended to form a basis for subsequent studies into rapid local heating events. On the other hand, **Paper VI** takes the form of a review paper, where the current best practices in rail machining were investigated. Rail grinding has been performed in field for several decades by now and the consensus is that it is a necessity; however, there are still some gaps in fundamental knowledge required. There is also a need for improved predictive models to determine the

influence of rail machining on the rail material. In this paper some key aspects of rail machining are highlighted as possible development areas: the effect of thermal power on the material properties in the surface layers of the rail head should be investigated. The study in **Paper V** built on this by focusing on rail grinding. Although the laboratory experiments cannot be performed in a manner that is representative of rail grinding in practice, this study provides insights into the effects of grinding on rail materials. Two rail grades, R260 and R350HT, were compared and both planar grinding and faceted grinding were investigated. This allowed for evaluation of the depth of martensitic transformation as well as the tempering effects of subsequent grinding passes.

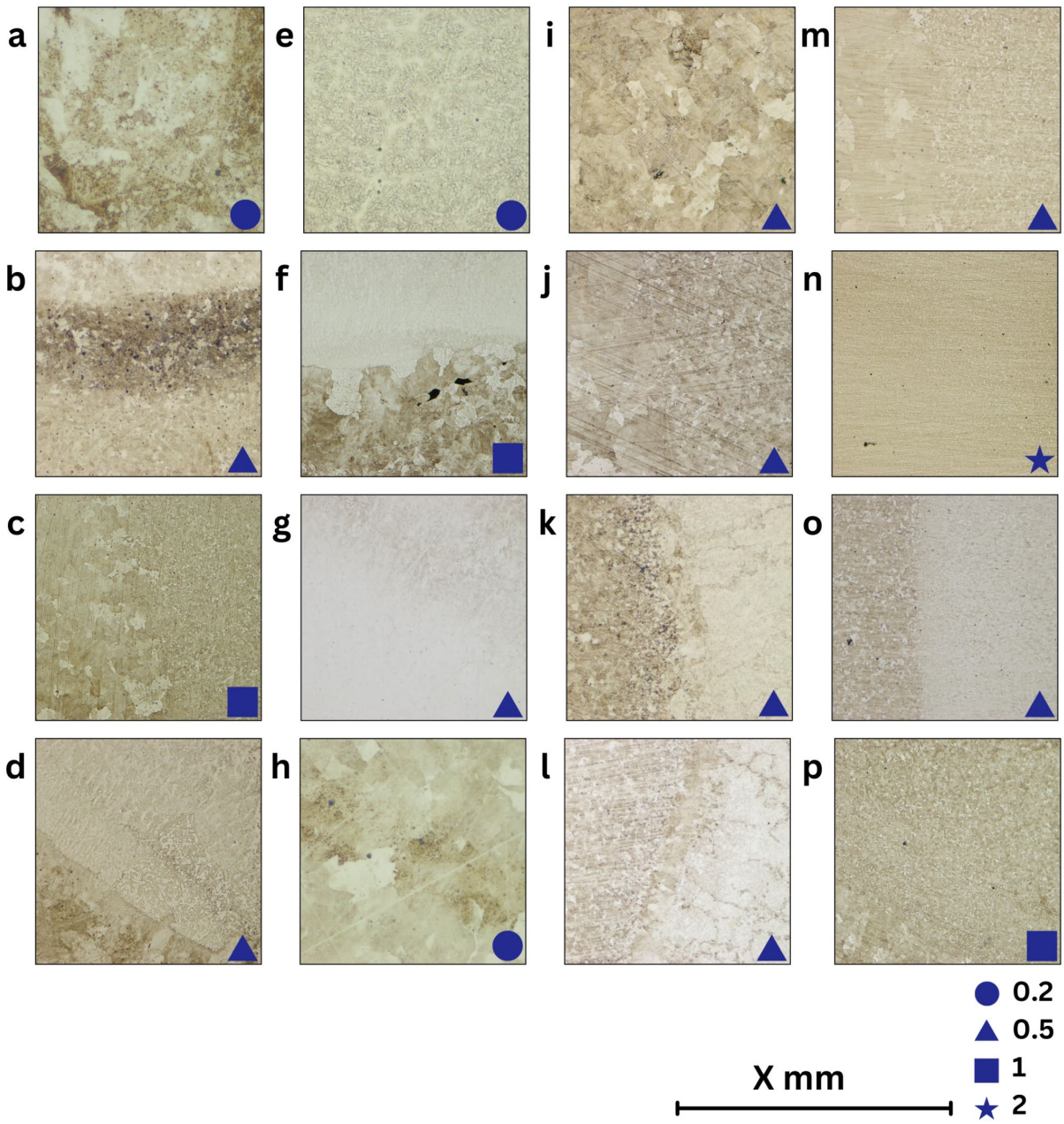

***Figure 26**: Micrographs taken at various locations as identified on Figure 25. Since the scaling of the images were different, the scale is identified with a shape, where X is either 0.2 mm, 0.5 mm,1 mm or 2 mm.*

CONCLUDING REMARKS

6.1. Research objectives as addressed in appended papers

This thesis work investigated the thermo-mechanical behaviour of pearlitic and near-pearlitic railway steels during high temperature processes. The main research objectives as stated in Section 1.3 were: (numbered for reference in this summary section)

RO.1: Experimentally simulating the effect of severe block braking on near-pearlitic railway wheel steel (ER7T) behaviour and microstructure by exposing material to various thermo-mechanical loading cycles with different peak temperatures and degrees of restriction of thermal dilatation.

RO.2: Characterisation of the effect of rapid local heating and cooling events on the microstructure and residual stress state, comparing near-pearlitic railway wheel steel (ER7T) and pearlitic rail steel (R260).

RO.3: Review the implications of maintenance processes of pearlitic railway steel regarding deterioration due to thermal and thermo-mechanical loads.

Each of the included studies aimed to address at least one of these research objectives. Below is a short summary of how each appended papers relates to the research objectives:

- **Paper I** provided insight into the material behaviour of near-pearlitic railway wheel steel during severe block braking, representing a slow heating and cooling cycle. The thermo-mechanical behaviour was investigated by varying the degree of thermal dilatation restriction. It was shown that thermo-mechanical loads do not have severe consequences for the mechanical properties (i.e. strength and hardness) of the railway wheel rim material; however, significant tensile residual stresses would remain in the hoop direction of the wheel after severe overheating. This directly addresses RO.1 as stated above.
- **Paper II** considered the relation between thermo-mechanical loading and microstructural evolution in near-pearlitic railway wheel steel. Hardness and spheroidisation quantification results showed that the fine-pearlitic microstructure in the wheel rim is sensitive to thermo-mechanical loading with a peak temperature of 650 °C, and an increase in compressive stress during the heating cycle correlates with lower degrees of pearlite spheroidisation at high temperatures. This paper addresses RO.1, but also provides valuable insight in the material behaviour that can be used to address RO.3. This thesis work provided evidence that railway steel R260 and ER7T wheel rim material show similar trends in material behaviour, specifically

considering the spheroidisation of pearlite, which can inform railway and rail wheel tread maintenance procedures.

- **Paper III** described the development of a new numerical model for severe block braking through improvements to the constitutive material model and careful calibration including the results of thermo-mechanical experiments, complemented by isothermal test results. This follows on RO.1. Furthermore, based on the findings from Paper II and this thesis work, the modelling framework could be used as a predictive tool for the material behaviour during other thermo-mechanical load cases, like maintenance processes resulting in localised heating (addressing RO.3).
- **Paper IV** investigated the effect of rapid local heating by laser scanning on hardness, microstructure and residual stress development in railway steels. Near-pearlitic wheel steel was compared to pearlitic rail steel; evaluation of the final martensitic microstructure revealed distinct differences in the final residual stress states. This study addresses RO.2 directly; it can also be used to develop improved maintenance strategies for both rail and railway wheels, addressing RO. 3.
- **Paper V** focussed on the effect of parameter variation during rapid heating and cooling events (specifically, grinding operations). No significant differences in the martensitic transformation were noted between standard and premium rail grades. This study also provided insight into martensite formation and tempering, which could inform operational and maintenance processes that result in repeated rapid local heating. The findings from this study supports RO.2 and RO.3 as stated above.
- **Paper VI** is a review of the current state-of-the-art of railway maintenance and highlights the need for improved understanding of fundamental material behaviour and predictive tools. The work in this thesis showed that predictive tools developed for operational conditions could be utilised for maintenance processes. This directly addresses RO.3, but also shows the importance of findings from RO.1 and RO.2 to address existing knowledge gaps.

6.2. Future work

This doctoral thesis project aimed to improve the understanding of high temperature processes on both rail and railway wheel steel. The following focus areas are suggested for future studies:

- The investigation into the thermo-mechanical behaviour of railway steel have shown complex residual stress states can develop as a result of the combined loadings. It could be of interest to investigate these residual stresses more extensively. An ongoing study into the residual stresses at grain level can be used to explain the global residual stress behaviour.

- The investigating of transformation plasticity to identify the material behaviour upon transformation between pearlite and austenite.
- Improved characterisation and simulation of martensitic transformations. The martensite formation during rapid cooling is considered a detrimental effect of high temperature processes like rail grinding. Although martensite is a very common microstructure, the understanding of how it forms under thermo-mechanical loads and how this affects its properties are still limited.

Acknowledgements

I would like to start by thanking the CHARMEC research group and our industrial partners for their financial support and invaluable practical perspective. I would like to specifically thank Voestalpine, Lucchini Sweden AB and Lucchini RS (especially Andrea Ghidini) for supplying the material used for testing.

Professor Johan Ahlström: your support and encouragement made this work possible. Thank you for always being willing to help and showing interest on a professional and personal level. I hope you know how much I have appreciated your guidance as my supervisor. Thank you! I am also grateful to my collaborators for pleasant and fruitful discussions; particularly my co-supervisor Professor Magnus Ekh, Björn Andersson, Professor Lennart Josefson, Professor Tore Vernersson and Eric Landström. To Professor Anders Ekberg and Dr. Björn Paulsson: I owe in large part my interest in this field to you!

A special thanks to William Hearn, Sri Bala Aditya Malladi and Dr. Zhuoer Chen from the Centre for Additive Manufacture – Metal (CAM2), as well as Ove Wahlbeck at Alpha Laser GmbH for their insights and assistance with the laser scanning experiments. Also, to Dr. Eric Tam, Prof. Christer Persson, Prof. Fang Liu and Roger Sagdahl for invaluable advice and guidance along the way. A special mention to the students I have worked with during the past five years - Arda Baytaroglu, Bastien Moreno, Caroline Andersson, Maria Börjesson and Per Emanuelsson. Thank you for all your assistance along the way; I learnt so much from each of you.

On a more personal note, thank you to my colleagues and friends (both past and present) at the Department of Industrial and Materials Science for good fika discussions and fun hallway banter. To my "Swedish family" – you know who you are (yes, I am scared to list names because it would take a page and I might miss someone). I love every one of you and appreciated every coffee, dinner, or doorway chat. Finally, thank you to my South African family and friends for the love, support, and prayers – I love you to the moon and back!

Last, but certainly not least: a special thank you to my hartsmense. My parents, Ertjies and Joan, for being my sounding boards, proofreaders and personal draughting service when my CAD skills let me down. Mamma, thank you for being my safe haven and pillar of strength in probably the most trying times of my life. And to my amazing siblings, Juvan, Tiaan, Shezanne, Monique and Sarita, for being there for me and loving me just as I am.

Gothenburg, May 2024
Erika Steyn

References

[1] Coles JM, Hibbert FA, Orme BJ, Pettit M, Rushton D, Switsur VR. *Prehistoric Roads and Tracks in Somerset, England: 3. The Sweet Track*. Proceedings of the Prehistoric Society 1973;39:256–293. https://doi.org/10.1017/S0079497X00011683.

[2] European Commission. *EU transport in figures - statistical pocketbook*. 2021. ISBN: 92-76-40101-8

[3] Directorate-General for Mobility and Transport. N*ew transport proposals target greater efficiency and more sustainable travel.* European Commission News 2021.

[4] Press release: *Council adopts European climate law.* Brussels: Council of the EU. 2021.

[5] Directorate-General for Transport and Mobility. *Unit C4 - Rail Safety and Interoperability. Europe's Rail Joint Undertaking - Master Plan (draft)*. Brussels: European Commission. 2021.

[6] Zhou K, Ding H, Steenbergen M, Wang W, Guo J, Liu Q. *Temperature field and material response as a function of rail grinding parameters.* International Journal of Heat and Mass Transfer 2021;175. https://doi.org/10.1016/j.ijheatmasstransfer.2021.121366.

[7] Uhlmann E, Bobyr M, Borodiy Y, Lypovka P, Protsenko P, Thalau J. *Influence of railway-track grinding on the track material condition and tribological behaviour.* Advanced Materials Letters 2019;10(7):449–454. https://doi.org/10.5185/amlett.2019.2234.

[8] Skyttebol A. *Continuous Welded Railway Rails: Residual Stress Analyses, Fatigue Assessments and Experiments.* Doctoral dissertation. Chalmers University of Technology, Gothenburg, 2004.

[9] Josefson BL, Bisschop R, Messaadi M, Hantusch J. *Residual stresses in thermite welded rails: significance of additional forging.* Welding in the World 2020;64(7):1195–1212. https://doi.org/10.1007/s40194-020-00912-4.

[10] The European Union horizon 2020 program. WRIST – Innovative Welding Processes for New Rail Infrastructures. Grant Agreement 636164, 2015.

[11] Simon Niederhauser. *Laser cladded steel – microstructures and mechanical properties of relevance for railway applications.* Doctoral dissertation. Chalmers University of Technology, Gothenburg, 2005.

[12] The European Union horizon 2020 program. INFRASTAR - Innovation and Networking for Fatigue and Reliability Analysis of Structures - Training for Assessment of Risk. Grant Agreement 676139, 2020.

[13] Ahlström J. *Thermal and Mechanical Behaviour of Railway Wheel Steel*. Doctoral dissertation. Chalmers University of Technology, Gothenburg, 2001.

[14] Jergéus J. *Martensite formation and residual stresses around railway wheel flats.* Proc Instn Mech Engrs, Part C, Vol 212(1). 1998. https://doi.org/10.1243/0954406981521051

[15] Cvetkovski K. *Influence of thermal loading on mechanical properties of railway wheel steels.* Doctoral dissertation. Chalmers University of Technology, Gothenburg, 2012. ISBN 978-91-7385-750-5

[16] Jessop C. *Damage and defects in railway materials: influence of mechanical and thermal damage on crack initiation and propagation.* Doctoral dissertation. Chalmers University of Technology, Gothenburg, 2019. ISBN 978-91-7905-132-7

[17] Ahlström J. *Modelling of properties and damage in wheel and rail materials* (CHARMEC MU30). Project report. 2021.

[18] Srivastava JP, Sarkar PK, Ranjan V. *Effects of thermal load on wheel–rail contacts: A review.* Journal of Thermal Stresses 2016;39(11):1389–1418. https://doi.org/10.1080/01495739.2016.1216060

[19] Lee HC, Jin YG, Lee YH, Son IH, Lee DL, Im YT. *Process design of high-strength bolt of fully pearlitic high-carbon steel.* Journal of Materials Processing Technology 2010;210(14):1870–1875. https://doi.org/10.1016/j.jmatprotec.2010.06.017

[20] Borchers C, Kirchheim R. *Cold-drawn pearlitic steel wires*. Progress in Materials Science 2016;82:405–444. https://doi.org/10.1016/j.pmatsci.2016.06.001

[21] Ono K. *Size effects of high strength steel wires.* Metals, 9(2), 2019. https://doi.org/10.3390/met9020240.

[22] Tashiro H, Tarui T. *State of the art for high tensile strength steel cord.* Steel Research Laboratories, Kamaishi Works. Nippon Steel Technical Report No. 88. 2003. pp.87–91.

[23] EN 13262: *Railway applications - Wheelsets and bogies - Wheels - Product requirements.* Brussels: CEN - European Committee for Standardization: 2020.

[24] EN 13674-4: *Railway applications – Track – Rail – Part 4: Vignole railway rails from 27 kg/m to, but excluding 46 kg/m.* Brussels: CEN - European Committee for Standardization; 2019.

[25] Diener M, Ghidini A. *Materials for heavy haul solid wheels: New experiences.* Proceedings of the Institution of Mechanical Engineers, Part F: Journal of Rail and Rapid Transit, 224(5), 2010, pp. 421–428. https://doi.org/10.1243/09544097JRRT356.

[26] Mädler K, Bannasch M. *Materials used for Wheels on Rolling Stock.* Brandenburg-Kirchmöser, Germany: Deutsche Bahn AG, Technical Centre. Technical Report; 2006. pp. 428-435

[27] Arnaiz Merino R. *Development of Railway Wheels with Alternative Materials and Production Processes.* Master thesis. Graz University of Technology, 2015.

[28] Pointner P, Joerg A, Jaiswal J. *INNOTRACK D4.1.5GL: Definitive guidelines on the use of different rail grades*. 2006.

[29] *Heat Treated High Performance Rail 350HT HSH*, voestalpine Schienen GmbH: Catalogue, 2022.

[30] EN 13674-1: *Railway applications - Track - Rail - Part 1: Vignole railway rails 46 kg/m and above.* Brussels: CEN - European Committee for Standardization; 2017.

[31] Porter DA, Easterling KE. *Phase Transformations in Metals and Alloys*. Boston, MA: Springer US; 1992. https://doi.org/10.1007/978-1-4899-3051-4.

[32] Bhadeshia H, Honeycombe R. *Chapter 2: Strengthening of Iron and Its Alloys*. Steels: Microstructure and Properties, Elsevier; 2017, pp. 23–57. https://doi.org/10.1016/B978-0-08-100270-4.00002-0.

[33] Hackney SA, Shiflet GJ. *Pearlite growth mechanism*. Acta Metallurgica 35(5):pp.1019–1028, 1987. https://doi.org/10.1016/0001-6160(87)90049-6.

[34] Nikas D, Ahlström J, Malakizadi A. *Mechanical properties and fatigue behaviour of railway wheel steels as influenced by mechanical and thermal loadings*. Wear, 366–367:pp.407-415, 2016. https://doi.org/10.1016/j.wear.2016.04.009.

[35] Van Vlack LH. *Elements of Materials Science and Engineering*. 6th ed. Ann Arbor, Michigan: Addison-Wesley Publishing Company; 1989.

[36] Chattopadhyay S, Sellars CM. *Kinetics of pearlite spheroidisation during static annealing and during hot deformation*. Acta Metallurgica, 30(1):pp. 157–70, 1982. https://doi.org/10.1016/0001-6160(82)90055-4.

[37] Bhadeshia H, Honeycombe R. *Chapter 2: Iron-Carbon Equilibrium and Plain Carbon Steels*. 4th ed. Elsevier Ltd; 2017. pp.59-100. https://doi.org/10.1016/b978-0-08-100270-4.00003-2.

[38] Nutal N, Gommes CJ, Blacher S, Pouteau P, Pirard JP, Boschini F, et al. *Image analysis of pearlite spheroidization based on the morphological characterization of cementite particles.* Image Analysis and Stereology 29(2):pp.91-98. 2010. https://doi.org/10.5566/ias.v29.p91-98.

[39] Zhang M-X, Kelly PM. *The morphology and formation mechanism of pearlite in steels.* Materials Characterization 60(6):pp.545–554, 2009. https://doi.org/10.1016/j.matchar.2009.01.001.

[40] Tian YL, Kraft RW. *Mechanisms of Pearlite Spheroidization*. Metallurgical Transactions A 18(8):pp.1403–1414, 1987. https://doi.org/10.1007/BF02646654.

[41] Umemoto M, Todaka Y, Tsuchiya K. *Mechanical properties of cementite and fabrication of artificial pearlite*. Materials Science Forum. vol. 426-432. 2003. pp.859-864 https://doi.org/10.4028/www.scientific.net/MSF.426-432.859

[42] Bhadeshia H, Honeycombe R. *Chapter 5: Formation of Martensite*. Steels: Microstructure and Properties, Elsevier; 2017, p. 135–77. https://doi.org/10.1016/b978-0-08-100270-4.00005-6.

[43] Malheiros LRC, Rodriguez EAP, Arlazarov A. *Mechanical behavior of tempered martensite: Characterization and modeling*. Materials Science and Engineering: A. 706(8):pp.38–47, 2017. https://doi.org/10.1016/j.msea.2017.08.089.

[44] Speich GR, Leslie WC. *Tempering of steel*. Metallurgical Transactions 3(5):pp.1043–1054, 1972. https://doi.org/10.1007/BF02642436

[45] Nikas D, Zhang X, Ahlström J. *Evaluation of local strength via microstructural quantification in a pearlitic rail steel deformed by simultaneous compression and torsion*. Materials Science and Engineering A 737:pp.341–347, 2018. https://doi.org/10.1016/j.msea.2018.09.067.

[46] Umemoto M, Liu ZG, Takaoka H, Sawakami M, Tsuchiya K, Masuyama K. *Production of bulk cementite and its characterization.* Metallurgical and Materials Transactions A 32A:pp.2127 2131, 2001. https://doi.org/10.1007/s11661-001-0024-y.

[47] Bhadeshia HKDH. *Cementite*. International Materials Reviews 65(1):pp.1–27, 2020. https://doi.org/10.1080/09506608.2018.1560984.

[48] Duka E, Oettel H, Dilo T. *Connection between micro and macro hardness pearlitic-ferritic steel*. AIP Conference Proceedings, 2012, p. 47–51. https://doi.org/10.1063/1.4751563.

[49] Danilov VI, Gorbatenko V V., Zuev LB, Orlova D V., Danilova L V. *Luders deformation of low-carbon steel.* Steel in Translation 47(10):pp.662–668, 2017. https://doi.org/10.3103/S0967091217100035.

[50] Butler JF. *Lüders front propagation in low carbon steels.* Journal of the Mechanics and Physics of Solids, 10:pp.313–334, 1962. https://doi.org/10.1016/0022-5096(62)90003-0.

[51] Tsuchida N, Tomota Y, Nagai K, Fukaura K. *A simple relationship between Lüders elongation and work-hardening rate at lower yield stress*. Scripta Materialia 54:pp.57–60, 2006. https://doi.org/10.1016/j.scriptamat.2005.09.011.

[52] Mező TB, Barkóczy P. *Study on Static Strain Aging Kinetics of High-Carbon Steel Wires and Its Impact on High-Strength Steel Cords*. Metals 11:1684, 2021. https://doi.org/10.3390/met11111684.

[53] Gonzalez BM, Marchi LA, Fonseca EJ, Modenesi PJ, Buono VTL. *Measurement of dynamic strain aging in pearlitic steels by tensile test*. ISIJ International, 43(3):pp.428-432, 2003. https://doi.org/10.2355/isijinternational.43.428

[54] Sachdev AK. *Dynamic Strain Aging of Various Steels*. Metallurgical Transactions A. 13(10):1793–1797, 1982. https://doi.org/10.1007/BF02647835.

[55] Tsuzaki K, Matsuzaki Y, Maki T, Tamura I. *Fatigue deformation accompanying dynamic strain aging in a pearlitic eutectoid steel*. Materials Science and Engineering A 142:pp. 63–70, 1991. https://doi.org/10.1016/0921-5093(91)90754-B.

[56] Dowling NE. *Mechanical Behavior of Materials: Engineering methods for deformation, fracture and fatigue*. 4th ed. Pearson; 2013.

[57] ASM Handbook, Volume 19 - *Fatigue and Fracture*. Committee ASMIH. 1996. ISBN: 978-0-87170-385-9

[58] Kiani M, Fry GT. *Fatigue analysis of railway wheel using a multiaxial strain-based critical-plane index.* Fatigue & Fracture of Engineering Materials & Structures 41(2): pp.412–24, 2018. https://doi.org/10.1111/ffe.12697.

[59] Kapoor A. A re-evaluation of the life to rupture of ductile metals by cyclic plastic strain. Fatigue & Fracture of Engineering Materials and Structures 17(2):pp.201–19, 1994. https://doi.org/10.1111/j.1460-2695.1994.tb00801.x.

[60] Ahlström J, Karlsson B. *Modified Railway Wheel Steels: Production and Evaluation of Mechanical Properties with Emphasis on Low-Cycle Fatigue Behavior*. Metallurgical and Materials Transactions A, 40(7):pp.1557–1567, 2009. https://doi.org/10.1007/s11661-009-9846-9.

[61] Allison B. *Rolling-Contact Fatigue.* Failure Analysis and Prevention, vol. 11, ASM International; 2021, pp. 716–29. https://doi.org/10.31399/asm.hb.v11.a0006792.

[62] Paul SK. *A critical review of experimental aspects in ratcheting fatigue: microstructure to specimen to component*. Journal of Materials Research and Technology 8(5):4894–4914, 2019. https://doi.org/10.1016/j.jmrt.2019.06.014.

[63] Rider RJ, Harvey SJ, Chandler HD. *Fatigue and ratcheting interactions*. International Journal of Fatigue 17)7):pp.507–511, 1995. https://doi.org/10.1016/0142-1123(95)00046-V.

[64] Ekberg A, Sotkovszki P. *Anisotropy and rolling contact fatigue of railway wheels.* International Journal of Fatigue 23:pp.29–43, 2001. https://doi.org/10.1016/S0142-1123(00)00070-0.

[65] Eden HC, Garnham JE, Davis CL. *Influential microstructural changes on rolling contact fatigue crack initiation in pearlitic rail steels*. Materials Science and Technology 2(6)1: pp.623–629, 2005. https://doi.org/10.1179/174328405X43207.

[66] Socie D, Socie B. *Thermomechanical fatigue made easy*. Fatigue, 2007.

[67] Bhanu Sankara Rao K, Raj B. *Fatigue Testing: Thermal and Thermomechanical*. Encyclopedia of Materials: Science and Technology. 2001. pp.2999–3001. https://doi.org/10.1016/B0-08-043152-6/00534-9.

[68] Beck T, Håhner P, Kühn H-J, Rae C, E.E. A, Anderson H, et al. *Thermomechanical fatigue – the route to standardisation (TMF-Standard).* Novel Approaches to Improving High Temperature Corrosion Resistance. 2008, pp.384–99. https://doi.org/10.1533/9781845694470.3.384.

[69] Esmaeili A, Walia MS, Handa K, Ikeuchi K, Ekh M, Vernersson T, et al. *A methodology to predict thermomechanical cracking of railway wheel treads: From experiments to numerical predictions.* International Journal of Fatigue, 105:pp.71-85, 2017. https://doi.org/10.1016/j.ijfatigue.2017.08.003.

[70] Haidari A, Hosseini-Tehrani P. *Fatigue Analysis of Railway Wheels Under Combined Thermal and Mechanical Loads.* Journal of Thermal Stresses, 37(1):pp.34–50, 2014. https://doi.org/10.1080/01495739.2013.850967.

[71] Fesharaki M, Wang T-L. *The Effect of Rail Defects on Track Impact Factors*. Civil Engineering Journal, 2(9):pp.458–473, 2016. https://doi.org/10.28991/cej-2016-00000049.

[72] Okagata Y. *Design Technologies for Railway Wheels and Future Prospects*. Nippon Steel & Sumitomo Metal Technical Report 105. 2013.

[73] Andersson E, Berg M, Stichel S. *Rail vehicle dynamics.* Stockholm: KTH; 2007. ISBN: 9174152726

[74] Nikas D. *Influence of combined thermal and mechanical loadings on pearlitic steel microstructure in railway wheels and rails*. Doctoral dissertation. Chalmers University of Technology. Gothenburg, 2018.

[75] Lewis R, Olofsson U, editors. *Wheel—rail interface handbook.* 1st ed. Cambridge: Woodhead Publishing Limited; 2009. https://doi.org/10.1533/9781845696788.

[76] Kennedy FE. *Thermal and thermomechanical effects in dry sliding.* Wear 100(1-3):pp.453–76, 1984. https://doi.org/10.1016/0043-1648(84)90026-7.

[77] Barber J. *The conduction of heat from sliding solids.* International Journal of Heat and Mass Transfer, 13(5):pp.857–69, 1970. https://doi.org/10.1016/0017-9310(70)90131-6.

[78] Andersson R, Ahlström J, Kabo E, Larsson F, Ekberg A. *Numerical investigation of crack initiation in rails and wheels affected by martensite spots*. International Journal of Fatigue, 114:pp.238–251, 2018. https://doi.org/10.1016/j.ijfatigue.2018.05.023.

[79] Enblom R. *Deterioration mechanisms in the wheelï rail interface with focus on wear prediction: a literature review.* Vehicle System Dynamics, 47(6):pp.661–700, 2009. https://doi.org/10.1080/00423110802331559.

[80] Goo B-C, Seo J-W, Lee Y-J. *Effect of Welding Polarity on Mechanical Properties of Submerged Arc Welded Railway Vehicle Wheels.* Metals, 12:1381, 2022. https://doi.org/doi.org/10.3390/met12081381.

[81] AURORA Project. *Remanufacture of rail wheels*. TWI Global, Technical magazine: Network Rail Insight. 2022. [Accessed: 24 Aug 2022].

[82] Coo B-C, Lee Y-J. *Railway Vehicle Wheel Restoration by Submerged Arc Welding and Its Characterization.* Sci, 2, 33, 2020. https://doi.org/10.3390/sci2020033.

[83] Andersson B. *Modeling of phase transformations and cyclic plasticity in pearlitic steels. Doctoral dissertation.* Chalmers University of Technology, Gothenburg, 2024.

[84] Affeldt E, Loveday MS, Rinaldi Ricerca Sistema Energetico C. *Validated Code-of-Practice for Strain-Controlled Thermo-Mechanical Fatigue Testing.* European Commission - Joint Research Centre. Project No. GRD2-2000-30014; 2006. ISBN: 9279022164

[85] Vernersson T. *Temperatures at railway tread braking. Part 1: Modelling.* Proceedings of the Institution of Mechanical Engineers, Part F: Journal of Rail and Rapid Transit, 221(2):pp.167-182, 2007. https://doi.org/10.1243/0954409JRRT57.

[86] Vernersson T. *Temperatures at railway tread braking. Part 2: Calibration and numerical examples.* Proceedings of the Institution of Mechanical Engineers, Part F: Journal of Rail and Rapid Transit, 221(4):pp.429-442, 2007. https://doi.org/10.1243/09544097JRRT90.

[87] Teimourimanesh S, Vernersson T, Lundén R. *Modelling of temperatures during railway tread braking: Influence of contact conditions and rail cooling effect.* Proceedings of the Institution of Mechanical Engineers, Part F: Journal of Rail and Rapid Transit, 228(1):pp.93-109, 2014. https://doi.org/10.1177/0954409712465696.

[88] Walia MS, Esmaeili A, Vernersson T, Lundén R. *Thermomechanical capacity of wheel treads at stop braking: A parametric study*. International Journal of Fatigue, 113:pp.407–415, 2018. https://doi.org/10.1016/j.ijfatigue.2018.04.031.

[89] Esmaeili A, Ahlström J, Ekh M, Nikas D, Vernersson T. *Modelling of temperature and strain rate dependent behaviour of pearlitic steel in block braked railway wheels.* Railway Engineering Science, 29(4):pp.362–378, 2021. https://doi.org/10.1007/s40534-021-00244-z.

[90] Ahlström J, Kabo E, Ekberg A. *Temperature-dependent evolution of the cyclic yield stress of railway wheel steels*. Wear. 366–367:378–82, 2016. https://doi.org/10.1016/j.wear.2016.04.002.

[91] Hearn W. *Development of Structural Steels for Powder Bed Fusion - Laser Beam*. Doctoral dissertation. Chalmers University of Technology, Gothenburg, 2023.

[92] EOS M100 Datasheet, *Additive Manufacturing System for the Fast and Efficient Production of Delicate Metal Parts Metal Solutions*. OS GmBH: Munich: 2018.

[93] Cvetkovski K, Ahlström J, Karlsson B. *Thermal degradation of pearlitic steels: Influence on mechanical properties including fatigue behaviour.* Materials Science and Technology. 27(3):pp.648–654, 2011. https://doi.org/10.1179/026708310X520538.

[94] Nikas D, Ahlström J. *Characterization of microstructural changes in near pearlitic steels using orientation imaging microscopy - Influence of predeformation on local sensitivity to thermal degradation*. IOP Conference Series: Materials Science and Engineering 2015;89. https://doi.org/10.1088/1757-899X/89/1/012039.

[95] Andersson B, Steyn E, Ekh M, Josefson LB. *Simulation-Based Assessment of Railhead Repair Welding Process Parameters.* Submitted for International Publication (Paper IV), 2024.